JLAB-TN-17-055

C75 Cavity Specifications and Commissioning of the Prototype Cavity Pair

F. Marhauser, G. Ciovati, G. Cheng, R. Rimmer, A. Freyberger, E. Daly, M. Drury, T. Powers, J. Guo
2017-11-22

Contents

Abstract

This document details the design parameters and performance specifications for so-called C75 cavities. The new cavities shall push the energy gain of original CEBAF cryomodules to 75 MeV per module after refurbishment with minimal modifications to cavity and cryomodule components and therefore expenses. A brief background of the standard refurbishment program established in 2006 as well as rationales and implications due to the proposed C75 program are discussed. First commissioning results are provided for two C75 prototype cavities that have been installed in the most recent refurbished cryomodule C50-13 among six refurbished original CEBAF cavities.

1. C50 Cryomodule Refurbishment, Achieved Improvements and Needs for a C75 Program

In 2006 Jefferson Laboratory (JLab) initiated a cavity cryomodule (CM) refurbishment project with the aim to increase the energy gain of original, low-performing CMs from nominally 20 MeV (C20 CMs) to 50 MeV (C50) to enable a robust 6 GeV, five-pass operation of the Continuous Electron Beam Accelerator Facility (CEBAF) [1]. In the frame of the refurbishment process, a C20 CM is disassembled and each of the eight Original CEBAF (OC) five-cell Superconducting Radio Frequency (SRF) cavities removed and chemically re-processed by applying today's advanced techniques. Chemical re-processing refers to a light removal of the interior surface (25 µm target value), which establishes a new SRF surface interior. The removal has been carried out originally by buffered chemical polishing (BCP) and since March 2013 by electropolishing (EP) to aim for a smoother surface and improved performance. Presently, the cavity surface reprocessing includes EP, vacuum furnace heat treatment for hydrogen degassing, and high pressure rinsing (HPR) with ultra-pure water at a pump pressure around 90 bar, while ultrasonic degreasing is carried out before EP, heat treatment, and in preparation for HPR. Mechanical polishing/lapping of cavity flanges is routinely done as part of the refurbishment program to re-assure ultra-high vacuum compliance of the cavity flange connections.

Given the envisaged energy gain, the C50 refurbishment shall improve the accelerating field (E_{acc}) from nominally 5 MV/m to 12.5 MV/m, while the onset for field emission (FE) can be shifted to higher field levels or FE even eliminated in the operating regime. The latter implies the avoidance of new particulate contamination and thus requires strict clean-room assembly protocols. Furthermore, a chicane ('dogleg') in the fundamental power coupler (FPC) waveguide is implemented between the cavity and helium vessel flange. The dogleg – in contrast to the original straight waveguide – keeps the innermost (2 K) ceramic RF vacuum window out of sight for the electron beam, which eliminates the electrostatic charging on the ceramic. It otherwise can result into periodic arcing in the FPC and thus RF trips in the cavity as experienced in CEBAF, while the arcing rate increases with the field level once field emission is turned on [1]. Moreover, new (warm) alumina RF window ceramics for the cavity FPC's vacuum-to-air transition are installed in exchange of polyethylene windows, the mechanical cavity tuner (located inside the helium vessel) improved to reduce backlash, and damaged or worn components due to long-term radiation or mechanical wear, respectively, replaced. By 2011 ten C20 CMs (CM50-01 through CM50-10) had been successfully refurbished with the achieved improvements summarized in Table 1 [1]. Three further CMs (CM50-11 through CM50-13) have been refurbished and commissioned by 2013, 2016 and 2017, respectively.

Despite the success of the C50 refurbishment progress, a steady gradient loss has been observed in CEBAF with a loss rate of 34 MeV per pass per year based on operational data from 1995-2016 (not yet including losses from new C100 CMs) [2]. The conclusion was that an annual refurbishment of a C20 into a C50 CM would be insufficient to maintain the energy reach of 2.2 GeV per pass over time for the 12 GeV era of CEBAF. It also has to be considered that the energy gain achievable due to the refurbishment will reduce over time since the lowest-performing C20 CMs are usually replaced first. Since the annual gradient gain must exceed the estimated gradient loss, the required energy gain has been evaluated to be at least 64 MeV/year. This consideration led to the proposal of a C75 program in 2015, i.e. to further enhance the energy gain of C20 CMs to 75 MeV by implementing new in exchange of old cavities. To practically evaluate the risks of such an endeavor as early as possible, a C75 cavity pair has been built at JLab and installed and commissioned as part of CM50-13 among six standard C50 cavities. The results will be detailed later (cf. section 8).

Table 1: Improvements achieved for ten refurbished C20 CMs housing a total of 80 cavities (CMs C50-01 through C50-10). The operational limitations in CEBAF are listed at the bottom of the table. Data have been summarized from ref. [1] (status 2011)

Description	Unit	C20 cavities	C50 Cavities
# of cavities with $E_{acc} \geq 12.5$ MV/m as commissioned		8/80 (10 %)	69/80 (≈86 %)
Average maximum E_{acc} during commissioning	MV/m	9.1*	14.4
Average increase of E_{acc} after refurbishment	MV/m	-	5.4
Average usable E_{acc} in CEBAF**	MV/m	-	12.2
# of cavities with usable $E_{acc} \geq 12.5$ MV/m in CEBAF		-	53/80 (≈66 %)
Cavities with field emission radiation		71	36
Average field emission onset field	MV/m	6.9	11.6
Operational limitations (# of cavities)			
Quench		-	65
Available Power Limit		-	8
Waveguide Vacuum Fault		-	3
Reflected Power		-	2
Warm window temperature fault		-	1
Waveguide arcs		-	1

* Original commissioning in 1992-1993, ** The Low Level RF control limited the useable E_{acc} to 13.5 MV/m, though E_{acc} as high as 20 MV/m could be reached in C50 cavities.

2. C75 Cavity Program

The active length (L_{act}) of a five-cell cavity (iris to iris) at 1.5 GHz is ≈ 0.5 m based on the wavelength. This may slightly change depending on the cavity design and fabrication tolerances. At 75 MeV energy gain this mandates a usable field of E_{acc} = 18.75 MV/m, which is typically beyond the reach of the refurbished OC cavities per Table 1. It is also higher than the nominal field (E_{acc} = 17.86 MV/m) required for upgrade Low Loss (LL) seven-cell CEBAF cavities aiming for 100 MeV per CM (C100).

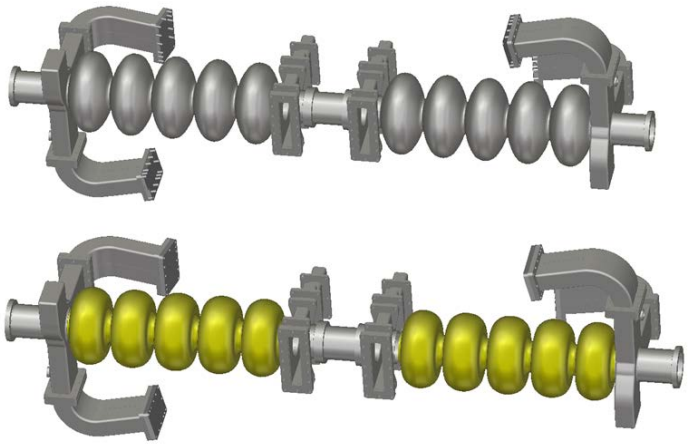

Figure 1: 1497 MHz OC cavity pair (top) versus C75 cavity pair (bottom) utilizing HC cavity cells as highlighted. The C20 HOM waveguides (two per cavity) and the FPC waveguide are recycled for C75 cavities. Not shown are mechanical stiffeners between cells and endgroups for the C75 cavity that shall provide the same structural integrity as a C20 cavity.

To achieve the comparatively high operational field, it has been proposed to exchange the old OC cavity cells with fresh so-called High Current (HC) five-cell cells [3]. As the most economic – since least-invasive – approach it has been decided to only replace the cavity cells but recycle C20 endgroups. The cell modification is illustrated for a cavity pair assembly model in Fig. 1. Each cavity pair will share a common helium vessel reused from C20 cryomodules. In this manner most of the C20 cavity and cryomodule hardware can be recycled and refurbishment expenses minimized. The cavity endgroups consist of a beam tube and the rectangular FPC waveguide section on one cavity end and two rectangular Higher Order Mode (HOM) damping waveguides (plus stub) on the other end (see Fig. 2).

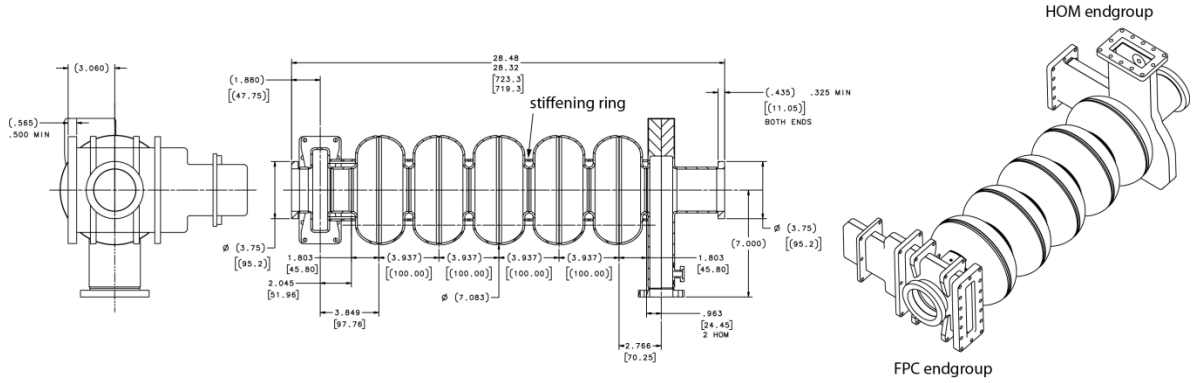

Figure 2: Assembly drawing of the C75 five-cell cavity with stiffening rings.

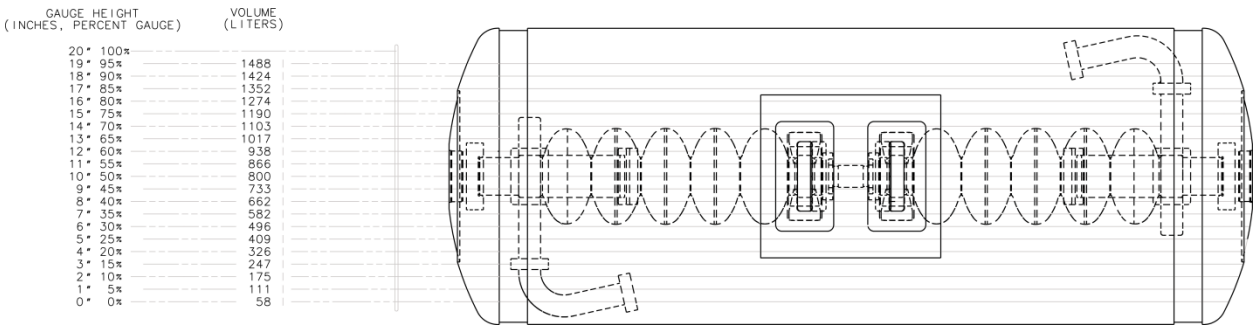

Figure 3: View of a C20 cavity pair within its helium vessel, which is made from stainless steel. Fractional amounts of the liquid helium level and corresponding volumes are denoted on the left revealing that at some portion of the upper HOM waveguide is never fully immersed in the helium bath.

The deviation of the shape contour between a C20/C50 and a C75 cavity is highlighted in Fig. 4 for a bare five-cell cavity. Due to the straight side walls of the HC cells, the cavity is mechanically less stiff.

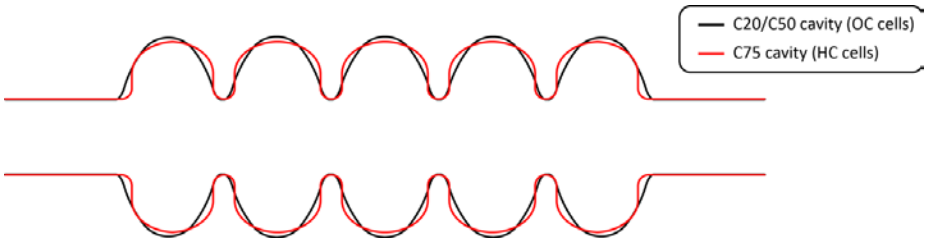

Figure 4: Comparison of the OC cells with HC cells by means of a bare five-cell cavity model.

Therefore the C75 cavities are reinforced by stiffening rings between the cells as well as between end half-cells and endgroups as drawn in Fig. 2. The radial position of the stiffening rings with respect to the cavity center has been optimized numerically by finite element analysis to yield a mechanical stiffness comparable to an OC cavity [4], resulting in a location at 48 mm radius from the cavity axis. This was important to guarantee full operational compatibility with the existing mechanical tuner mechanism. Experimental tests have been carried out to verify the stiffness and proper tuner operation. Hereby the tuner hysteresis curve (within $\approx \pm 250$ kHz), the cavity tuning sensitivity (in the linear regime with $|\Delta f| > 50$ kHz), and the cavity stiffness have been validated at room temperature [5].

Note that the mechanical tuner is designed to operate within the helium vessel immersed in helium. The cavity will be left under compression to avoid backlash. The tuner presses on the end-cells via Aluminum holders surrounding the end-cells of a cavity. This also required a modification of the end-cell holders to comply with the HC cell contour. The modified tuner cell holders are highlighted in Fig. 5.

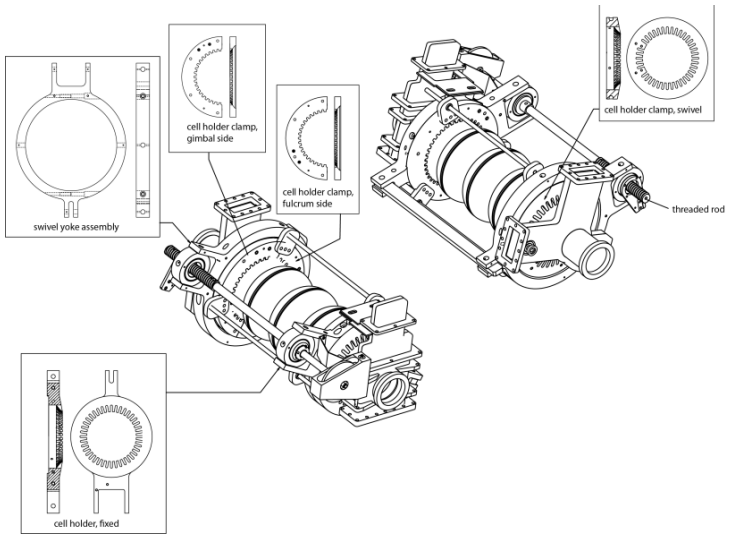

Figure 5: New tuner end-cell holders (made from aluminum) to adapt to the HC end-cell shape. The tuner is located within the helium vessel and operates at 2 K.

Moreover, it is known that the C20/C50 cavities have mechanical resonances allowing the HOM waveguide endgroup to swing. This could be verified for C75 cavities as part of a mechanical modal analysis (Fig. 6) [6]. To suppress such mechanical modes, HOM waveguide supports attached between the waveguide elbows and new magnetic shields (cf. section 7) are employed as shown in Fig. 7.

Geometry:	C75, full assembly	
Mode No.	f [Hz]	Description
1	41.93	HOM Waveguides
2	48.66	HOM Waveguides
3	74.09	Axial
4	91.70	Lateral Sway
5	119.0	Waveguides axial
6	146.4	FPC end sway

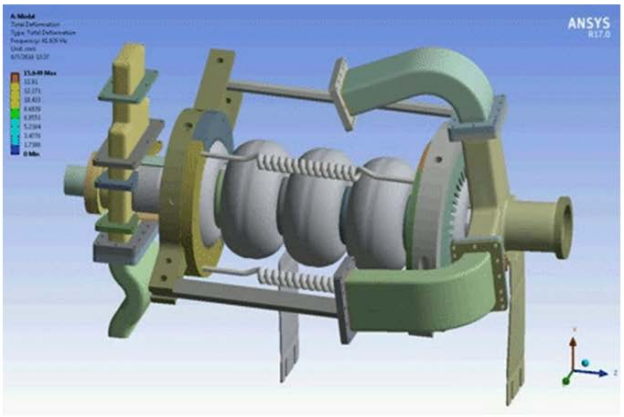

Figure 6: Mechanical modal analysis using ANSYS for a C75 cavity. Pictures and results are taken from ref. [6]. The first six mechanical resonances are listed in the Table (left). For the simulation the FPC waveguide with dogleg has been fixed, where it is nominally attached to the helium vessel (stiff flange note included for simplicity), ditto for cavity support plates. A symmetry plane is utilized to the left at the center of the cavity interconnecting beam tube adapter. The first two modes correspond to swinging modes of the whole HOM endgroup as depicted on the right.

A long-standing issue with the C20-style cryomodules has been achieving low residual magnetic fields at the cavity location. A systematic reduction of the cavity quality factor measured in the original CEBAF-style cryomodules, compared to the values measured in the vertical test cryostat was found. It was determined that a significant fraction of the additional losses result from high residual magnetic

field at the cavity. In order to mitigate such losses, an additional magnetic shield made of … mm thick Cryoperm® was designed to fit around the cavity. Openings in the shields were designed to allow helium flow to the cavity surface such that up to …W could be dissipated in the cavity before reaching He boiling regime. The new magnetic shields, shown in Fig. 7, were installed on all eight cavities in cryomodule C50-13.

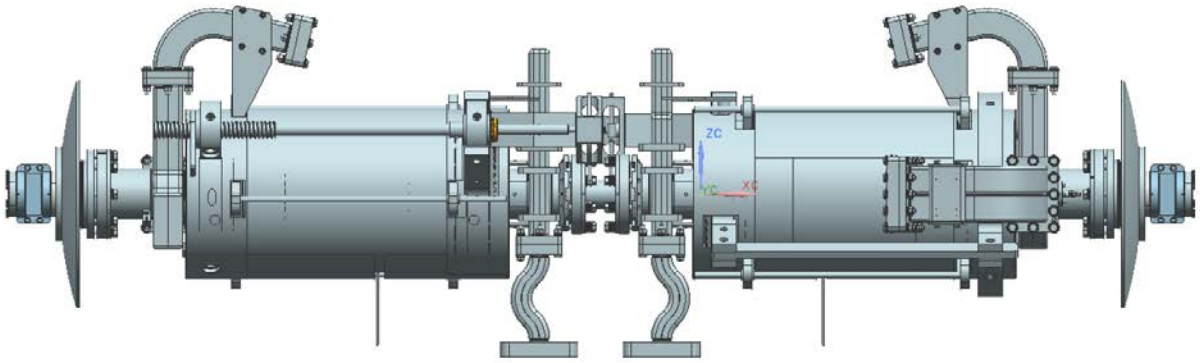

Figure 7: CAD model of cavity pair with new cavity magnetic shields employed since C50-13 and HOM waveguide supports, which have been installed for the first prototype C75 cavity pair in C50-13, but not yet for the C50 cavity pairs in C50-13. Picture has been taken from ref. [7].

3. Cavity Design Parameters

The relevant cavity parameters for various 1.5 GHz cavities designed at JLab are summarized in Table 2. Favoring HC cells over Low Loss (LL) and High Gradient (HG) shapes as a replacement for OC cells has been straightforward, not only since two 1.5 GHz HC cavity prototypes with HOM waveguide endgroups have been built and successfully tested vertically in the past at JLab (e.g. [3], [8]), but since the HC cell shape yields a similarly strong cell-to-cell coupling (k_{cc}) as the OC cell shape thanks to the same iris (and tube) aperture. This is essential for HOM-damping, when reusing the C20 waveguide couplers. In parallel, the surface electric and magnetic field enhancement ratios (E_{pk}/E_{acc} and B_{pk}/E_{acc}) are reduced by 4.3 % and 8.3 %, respectively. Furthermore, the dynamic (RF) heat dissipated in the cavity surface (~$(R/Q{\cdot}G)^{-1}$) at a given field is reduced by 9.5 % in comparison.

The LL cell shape has been specifically designed for C100 upgrade cavities to minimize cavity RF losses. Due to the small iris aperture it yields the lowest E_{pk}/E_{acc} and B_{pk}/E_{acc} values among the designs in Table 3. However, this comes at the expense of a very small cell-to-cell coupling of only 1.49%. Together with a larger number of cells it results in HOMs being stronger confined within the cavity, while even some propagating dipole modes are prone to tilt depending on fabrication tolerances as experimentally observed ([8], [9]). Avoiding the risks of elevating crucial HOM impedances, the LL cells – and for similar reasons the High Gradient (HG) cells – have a priori not been considered as suitable to replace the OC cavity cells.

Table 2: Relevant design parameters of existing 1.5 GHz JLab cavities exhibiting different cell shapes [1]

Parameter	Unit	Low Loss (LL) cavity	High Gradient (HG) cavity *	Original CEBAF (OC) cavity	High Current (HC) cavity
Number of cells		7	7	5	5
L_{act}	m	0.70	0.70	0.4999	0.4916
R/Q**	Ω	868.9	783.3	482.5	525.4
R/Q per cell	Ω	124.1	111.9	96.5	105.1
G	Ω	280.3	265.5	274.0	275.6
R/Q·G	Ω2	243553	207966	132205	144805
R/Q·G per cell	Ω2	34793	29709	26441	28961
E_{pk}/E_{acc}		2.17	1.89	2.56	2.45
B_{pk}/E_{acc}	mT/(MV/m)	3.74	4.26	4.56	4.18
k_{cc}	%	1.49	1.72	3.15	3.12
Tube ID	mm	70	70	70	70
Iris ID	mm	53	61.4	70	70
TE_{11} tube cutoff	GHz	2.51	2.51	2.51	2.51
TM_{01} tube cutoff	GHz	3.28	3.28	3.28	3.28

* designed and employed in prototype 'Renaissance' cryomodule together with LL cavities, ** $U_{eff}^2/(\omega * W)$

3.1 Fabrication Tolerances and Implications to Cavity Active Length and Field Flatness

The active length achievable of an as-built cavity depends on fabrication tolerances, while the target frequency must be met in parallel within specified tolerances in the Dewar (≈ ± 100 kHz). Fabrication tolerances arising from spring-back effects of the deep-drawn cells due to stress relief can be on the order of a few MHz already [10] and are compensated by cell trimming at the subassembly stage, but will inevitably lead to deviations from ideal cell dimensions denoted in drawings. Cell equator and iris weld shrinkages range typically within 0.4-1.0 mm as observed at JLab, but depend on the weld joint preparation/thickness as well as the procedure employed for electron beam welding (EBW). For instance, a single-pass full penetration weld is a standard joining technique of Nb sheets. Alternatively, partially penetrating welds from both the outside and inside (typically between 60-80% penetration each) can be performed as long as practically possible, which is deemed to yield a smoother weld under-bead and less risky concerning potential blow-through holes in equator welds. The latter however typically results in about twice the weld shrinkage due to the two EBW passes. The weld shrinkage is accounted for by leaving the half cells oversized appropriately after the final machining prior to EBW. Large thermal gradients encountered during EBW can further distort cells inadvertently with a resulting change in frequency at a given cell length. This is also true when stiffening rings are welded between cells. The amount of chemical or mechanical (CBP) removal and the non-uniformity of the removal from equator to iris is another factor that will change the cavity frequency notably. Material stress relieve during the heat treatment can also yield a cavity length change and corresponding frequency change as

[1] Simulations are based on fine-mesh 2D Superfish calculations for the full cavity except for the surface field enhancement ratios, which have been calculated for a mid-cell to further refine the mesh and improve the surface field accuracy. Depending on the simulation code and/or mesh resolution various parameters might have been published with slightly different values by other authors.

has been observed consistently for C100-type cavities built at JLab in the past [10].

It shall be noted that the OC cavity cells exhibit a design frequency of only ≈1489.5/1489.0 MHz in vacuum/air as verified numerically. Chemistry only lowers the frequency further. Additionally, the field flatness (*FF*) of the accelerating TM010 π-mode is not fully flat by design. This is illustrated in Fig. 8 for the C20 cavity with both endgroups attached as imported from a CAD model. This results in ≈92 %[2], whereby the field amplitude is affected most strongly on the HOM endgroup side. A similar 3D analysis for the C75 cavity resulted in *FF* ≈ 94 %, whereas the bare cavity per design (with nominal end-cell trimming) yields *FF* ≈ 98 %. It implies that the presence of the C20 HOM endgroup degrades the field flatness by ≈4 %, which practically must be compensated by bench tuning (plastic deformation of cells). The *FF* of an as-built cavity will typically be lower in reality than the design dimensions suggest[3] due to above described fabrication tolerances, which mandates even more bench tuning.

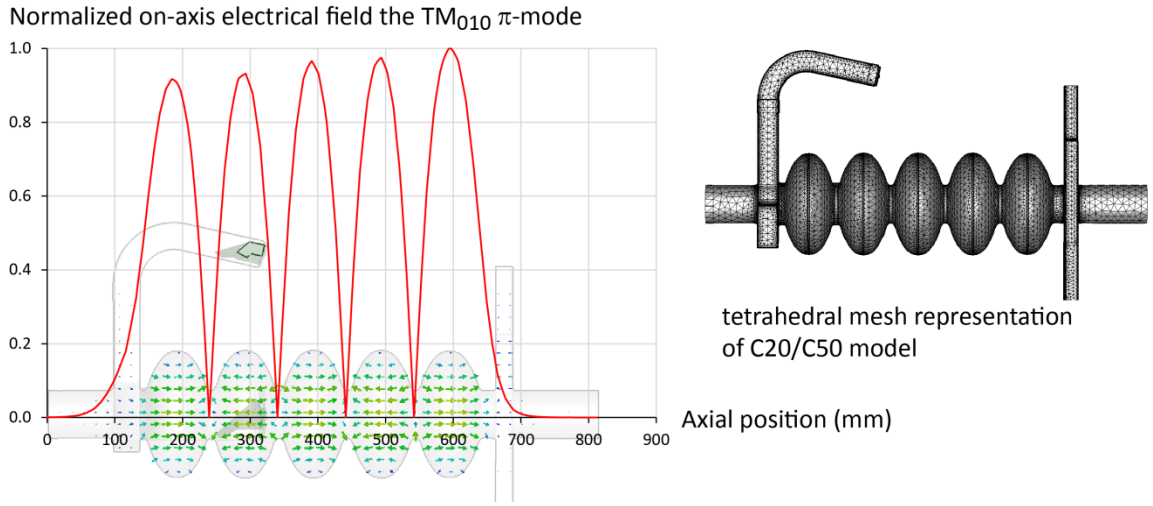

Figure 8: On-axis electrical field amplitude of the accelerating mode along the C20 cavity as calculated numerically using the Eigenmode solver of the CST Design Studio (CST) suite of codes.

The rather small frequency calculated for C20/C50 cavities has an implication to the cavity length. It is assumed that the vendor machined the half cells to the nominal size though this cannot be verified anymore (CEBAF drawings date back to the late 1980s). If so, this implies that the cavity as-built must have been stretched to raise the frequency to a proper target value.

Dimensional inspections at JLab routinely done for C50 cavity pairs using a coordinate measuring machine (CMM) indeed reveal that the length of the cavity pair from helium end dish to helium dish is much larger than designed. The control dimension is encircled in red in the cavity pair assembly drawing shown in Fig. 9. The findings of the survey are plotted in Fig. 10 revealing that almost all cavity pairs exceeded the toleranced margin. On average the cavity pairs are ≈14.9 mm larger than the nominal value. The central FPC to FPC waveguide separation (7.358" = 186.89 mm) is a rather strictly toleranced distance as the FPC flanges must be bolted to the helium vessel plate. This distance has been usually –

[2] The field flatness is defined here as the ratio of the minimum to maximum on-axis electrical field amplitude measured among individual cells along the cavity.

[3] For the as-built first three C75 prototype cavities a *FF* within 77-86% has been achieved [25].

not always – met within the dimensioned tolerance. The large length variations experienced are therefore assumed to be caused by deviations of the cavity cell lengths from ideal values and not from beam line length variations. It implies an active length deviation of ≈14.9/2 mm per cavity on average, which in turn equates to $\Delta f = +3.15$ MHz to be achieved by bench tuning. Hereby a tuning sensitivity of 420 kHz/mm is assumed[4]. This example validates that the C20 cavity design frequency is too low by several MHz and that the cavity length may err considerably after final bench tuning. Unlike for C100 CMs however, bellows are used in C20/C50 CMs between cavity pairs. This allows accepting cavities with relatively large length variations (flange to flange) for installation.

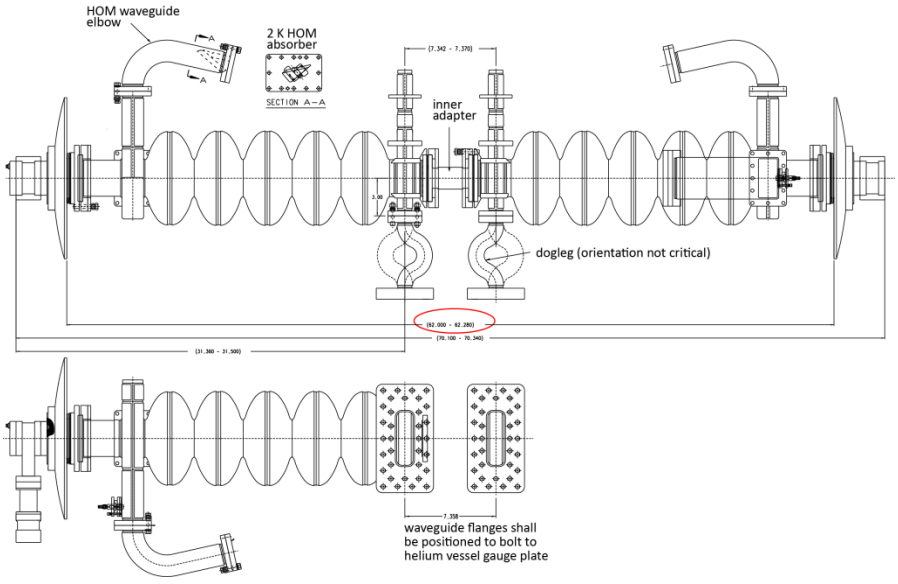

Figure 9: C50 cavity pair assembly drawing (all dimensions in inches). The highlighted values (red encircled) denote the distance as toleranced between helium end dishes (62.0-62.28").

[4] This value is only valid for the mechanical tuner compressing the whole cavity from both end-cells (cf. Table 2), but it is assumed to be on the same order to – but not identical with – the tuning sensitivity obtained during bench tuning, when individual cavity cells are plastically pushed or stretched by tuning plates inserted into irises around a cell. The true value depends on the actual cell deformation caused by bench tuning plates.

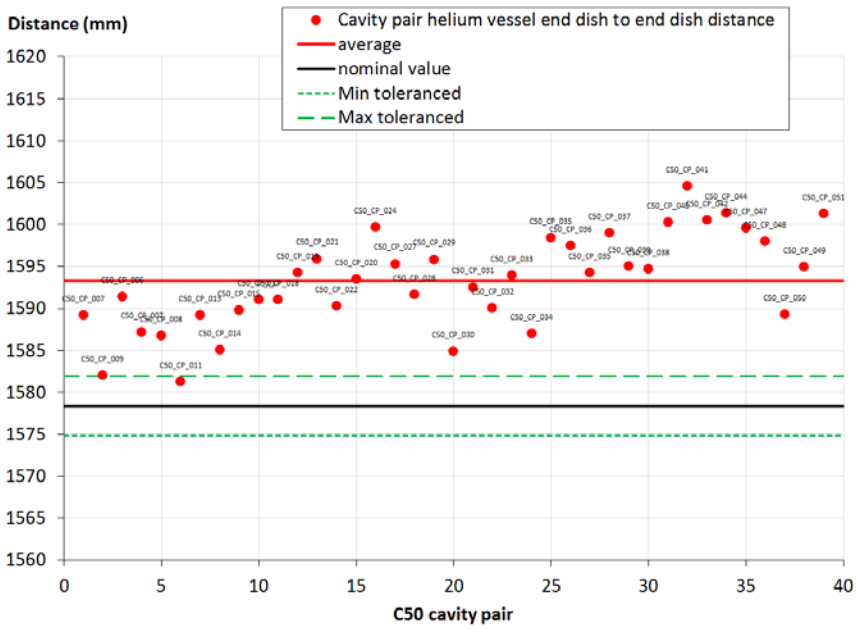

Figure 10: C20/C50 type cavity pair length dimensions as measured with a CMM from helium vessel end dish of one cavity to the helium vessel end dish of the adjacent cavity. The actual distance is typically much larger than the nominal value of 1578.36 mm ± 3.56 mm. The average length for 39 C50 cavity pairs is 1593.27 mm (Min = 1581.28 mm, Max = 1604.53 mm).

The question arises however whether the C75 cavities are fully compatible for assembly into a C20 cryomodule. Different to OC, LL, and HG cavities, the HC cavity is designed with both the mid-cells and end-cells exhibiting the same cell profile. Only a single deep-drawing die is needed for manufacturing. In order to achieve a flat accelerating mode per design, the end half-cells are trimmed shorter than the mid-cells before EBW. This eventually yields only L_{act} = 0.4916 m nominally instead of 0.5 m. The C75 cavity is thus shorter by ≈8.3 mm per design than an OC cavity (cf. contour plot in Fig. 4 further above). The nominal accelerating field required to meet 75 MeV energy gain is then actually 19.07 MV/m rather than 18.75 MV/m, which is not a negligible increase. The length of an OC cavity as-built is yet larger than 0.5 m as verified above. Experience with a HC five-cell cavity (HC002) showed that the nominal L_{act} could be met within 2 mm thanks to the better design frequency. The actual discrepancy of L_{act} between C20 and C75 cavities could therefore readily exceed 15 mm. On the hand, the FPC waveguide for C75 cavities is placed further away from the end-cell (≈20 mm). Assuming that the C20/C50 cavities are on average ≈14.9/2 mm longer, the length discrepancy between a C20/C50 and a C75 cavity is then ≈4.5 mm with the same endgroups in use (see Table 3). Eventually, the assembly length of a cavity can be more exactly controlled by adjusting the beam tube on one side of the cavity as done for C100 cavities. This is foreseen also for C75 cavities by customizing the beam tube length of an HOM endgroup, which however will add additional fabrication steps, i.e. cutting, machining, and EBW for the beam tube. The active, as-built cavity length deviation between C20/C50 and C75 cavities after tuning can thus be compensated and bears no risk for the cavity-pair assembly and alignment within an exisiting C20 helium vessel. Minor length discrepancies are accomodated by the bellows between cavity pairs. The installation length called out presently in the assembly drawing is included in Table 3.

Table 3: Cavity length comparisons between C20/C50 and C75 cavity

Parameter	Unit	C20/C50	C75
Nominal L_{act}	mm	499.9	491.6
Distance nearest end-cell iris to FPC center	mm	31.77	51.96 [a]
Actual L_{act} on average	mm	507.3 [b]	491.6 ± 3 [c]
Distance furthest end-cell iris to FPC center	mm	539.08	543.56
Assumed length increase compared to C20/C50	mm		+4.48
Controlling drawing number		1116-D-0001	JL0031321, Rev. B
Date		Oct. 1988	March 2016
Nominal installation length (flange to flange)	mm	720.73 ± 6.35 [d]	721.36 [e] ± 2
		717.55 ± 6.35 [f]	

[a] includes 20.19 mm added separation between FPC body and center cell, [b] +7.45 mm assumed per C50 cavity pair CMM analysis, [c] no firm fabrication tolerances exist yet, [d] specified in original CEBAF drawing as option 1 – raw, untuned cavity, [e] controlled by customizing beam tube on HOM endgroup side, [f] specified in original CEBAF drawing as option 2 – tuned, machined cavity

3.2 External Q of the Fundamental Power Coupler and Cavity Length Considerations

Setting the external Q (Q_{ext}) of the FPC is important to minimize the required RF generator power at a given beam loading, which must account for microphonic detuning of cavities, i.e. time-varying frequency detuning of the cavity due to external mechanical vibrations (e.g. transferred via ground motions or waveguides, vacuum pumps, helium pressure fluctuations etc.). One should take into account periodic microphonic excursions if manageable by the available RF power at the specified accelerating field to avoid RF cavity trips or to minimize RF trips to acceptably low rates. A larger microphonic detuning allowance comes at the expense of a higher RF power requirement. The Q_{ext} specifications for JLab cavities employed at CEBAF are summarized in Table 4.

Table 4. External Q specification for the various cavities operating in CEBAF

Cavity type Units	Nominal E_{acc} MV/m	Max. design E_{acc} MV/m	FPC Q_{ext} specification
C20	5	-	6.6e6 (± 20%)
C50	12.5	-	8e6 (± 25%)
C100	17.86	19.2 (+7.5%)	3.2e7 (± 20%)

The Q_{ext}-value of the FPC waveguide couplers is fixed by design since having no variable tuning mechanism. However, Q_{ext} is adjustable to some extent by means of a standard size (WR650) waveguide 3-stub tuner. These are routinely installed in CEBAF in the input power transmission lines external to the cryomodules. The 3-stub tuners house three plungers that move into the waveguide on the broad wall. Moving the plungers inside the waveguide creates a resonant circuit with a low quality factor between the stub tuner and the cavity that allows adapting the Q_{ext}-value. The plungers are each adjustable manually. The total tuning range achievable is theoretically 1-2 orders of magnitude ([11], [12]). It is experienced in CEBAF that the tuning to a higher Q_{ext} can be done more readily, while tuning to lower values – even by only a factor of 2 – creates excessive heating of the RF window verified by infrared

sensors [13]. It is therefore required to closely achieve the desired Q_{ext} before stub tuning, while the allowable margin is typically set to ± 20-25%. Yet, fabrication tolerances may cause the Q_{ext} to differ from the design value. In this case, the Q_{ext} is tuned on the bench by plastically deforming the FPC waveguide body – thus changing the coupling – on the broad wall close to the beam axis at the side of the FPC stub. For this purpose a dedicated tuning fork is utilized, which is connected at the top by a threaded rod (see Fig. 11). Spreading the prongs will squeeze the waveguide body and will increase the Q_{ext}-value. A slightly different, but similar tool is used to allow pulling on the waveguide body and lowering the Q_{ext}-value.

The C50 cavities have a slightly higher Q_{ext}-value specified than C20 cavities, which can be obtained by utilizing the tuning tool without an actual design modification. Exemplarily, Fig. 12 summarizes the Q_{ext}-values of the most recent 20 C20 cavities measured after disassembly as received on the tuning bench and measured after refurbishment passing the final tuning of the FPC body. At this point the cavity has been tuned to the target frequency at ambient conditions with a FF ≥ 95%.

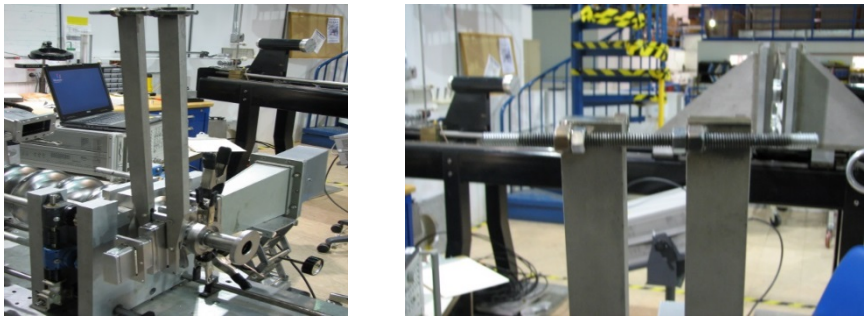

Figure 11: Tuning fork to mechanically deform the FPC body for *Qext* adjustment of the FPC.

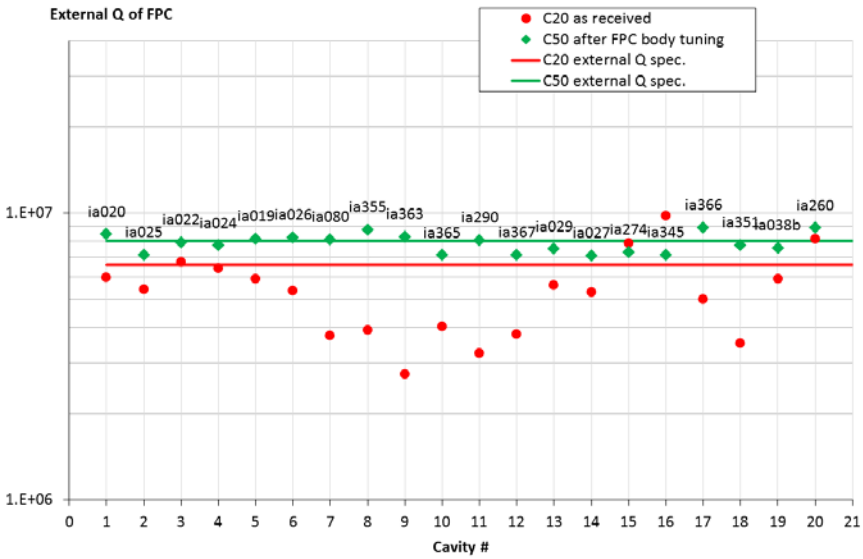

Figure 13: External Q-values as measured for OC cavities as received on the bench after disassembly from C20 cryomodules and after refurbishment passing the final tuning step by adjusting the FPC body. The lines represent the Q_{ext} specification for both cases. The cavity serial numbers are denoted. This ensemble of cavities is used in the most recent refurbished cryomodules (C50-11 to C50-13).

Several tuning steps are usually performed during the refurbishment process, e.g. cavity straightening – if necessary – will typically require a retuning of the Q_{ext}. The Q_{ext} specification for C50 cavities can eventually be met with good accuracy, while the distribution in Q_{ext}-values is about 5.2 smaller than for C20 cavities, which is a significant improvement in consistency. Table 5 summarizes the corresponding statistics. The Q_{ext} has been raised by ≈60 % on average after tuning the FPC body, but maximally by a factor of three. If a rather large Q_{ext} increase is required, the forces applied can be significant and could lead to a damage of the FPC body [14].

Table 5: Measured external Q-values for 20 OC cavities before and after refurbishment passing the final FPC body tuning step

Condition	$<Q_{ext}>$	σ	Min. Q_{ext}	Max. Q_{ext}	Specification
As received from CM	5.4e6	1.8e6	2.7e6	9.8e6	6.6e6
As tuned after refurbishment	7.9e6	0.6e6	7.1e6	8.9e6	8e6 ± 1e6

For the C75 cavities, the optimum Q_{ext} by design should be in the lower 1e7 range similar to C100 cavities in order to be more compatible with the 12 GeV operational beam conditions. The desired Q_{ext} will therefore be roughly two times higher than measured Q_{ext} for C20 cavities. Tuning the waveguide by plastic deformation is impeded by the stiffening rings between the end-cell and the FPC endgroup. The adaption to the much higher Q_{ext} has thus been considered by a larger separation of the FPC waveguide from the cavity end-cell rather than deforming the FPC body further (see Fig. 13). This design modification can be relatively easily achieved technically by welding an interconnecting Nb beam tube section to the existing FPC body. In preparation of a clean EBW joining fresh Nb sections, the FPC body is cut and weld joints machined for an additional, short interconnecting beam tube adapter welded to the body allowing for the weld shrinkage.

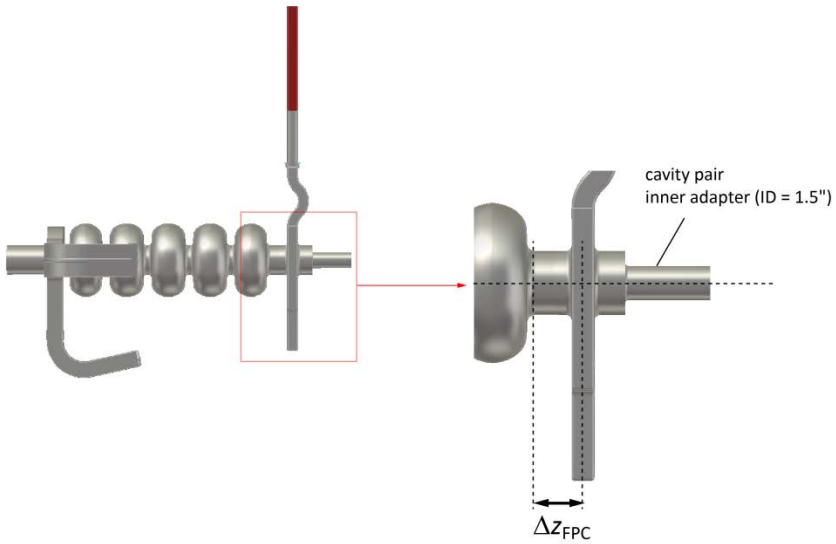

Figure 13: Illustration of the distance between the end-cell iris and the FPC waveguide center (Δz_{FPC}) for a C75 cavity as varied numerically to assess the external Q(Δz_{FPC}).

To assess the required beam tube separation, the Q_{ext}-value has been computed numerically for a C75 and a C20/C50 3D cavity model, respectively, as a function of the axial distance of the center of the

FPC waveguide to the nearby end half cell iris (Δz_{FPC}) as illustrated in Fig. 14. The computed results are plotted in a semi-logarithmic graph. The external Q follows the expected exponential dependency as a function Δz_{FPC} due to the coupling being facilitated via the exponentially-decaying (evanescent) fields of the accelerating mode in the beam tube. For the simulations the HOM endgroup and the FPC engroup with dogleg and RF window are included, while the cavity beam tube steps down according to the inner adapter (ID = 38.1 mm) that interconnects cavity pairs. This boundary condition had an influence of ≈25% on the external Q and is therefore not negligible. The two colored lines are exponential fit functions from slightly differing data (blue and orange symbols) that resulted from two Q_{ext}-values (Q_{lossy}, Q_{pert}) computed concurrently [15]. Hereby the open end of the FPC waveguide has been matched with a broadband, dissipative absorber placed at a sufficently large distance away from the beam tube. Using a dissipative material results in a complex solution with a traveling wave in the FPC[5]. The two data sets agree rather well and only deviate more significantly outside the interesting Q_{ext}-regime as the fit functions reveal. The black dots (Q_{pert} only) and correspnding fit function have been obtained for the C20/C50 cavity under the same conditions as for the C75 cavity. The red dots refer to the present Q_{ext} specifications for the C20 and C50 cavities, respectively, and reveal that these are higher than the design suggests at the nominal distance of $\Delta z_{FPC} \approx 31.8$ mm. For the C75 cavity, in order to increase Q_{ext} beyond 1e7 a separation of $\Delta z_{FPC} \geq 51.9$ mm is required. As a consequence, the beam tube between the end-cell and the FPC must be at least 20 mm longer than for C20/C50 cavities. An added ≈20 mm yields an overall cavity length increase (flange to flange) of ≈4.5 mm to C20/C50 cavities with the assumptions detailed above (cf. Table 3). The bellows between cavity pairs could accommodate this difference, though it is conceived to minimze any actual discrepancy by customizing the beam tube length of the HOM endgroup. A longer Δz_{FPC} implies a proportinally larger shortage of the beam tube.

[5] Alternatively one can set a waveguide boundary port to simulate a broadband match at the FPC end, however the Q_{ext} is computed still for a closed structure (electric and magnetic boundary), thus results in a standing wave in either case from which a traveling must be constructed to evaluate the Q_{ext}-value. It has been found that the corresponding results as calculated by CST are often unreliable when using this method.

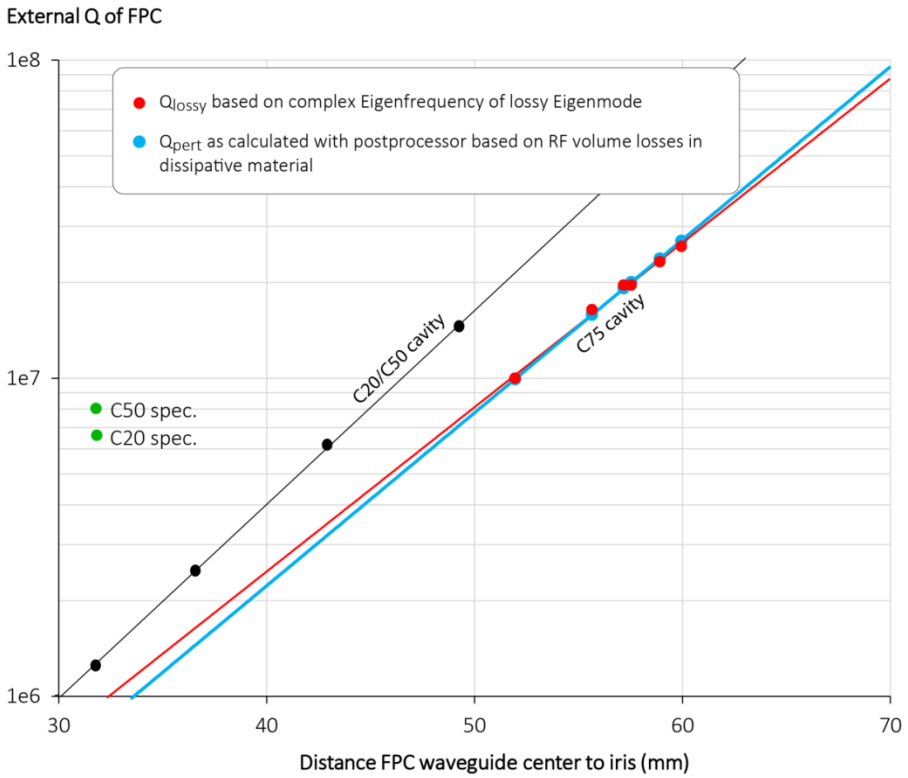

Figure 14: External Q of the FPC as simulated for a C75 and C20/C50 cavity, respectively, as a function of the distance of the FPC waveguide center to the nearby cavity end-cell iris (Δz_{FPC}). The complex Eigenmode solver of CST has been utilized resulting in two slightly different values as shown for the C75 cavity (blue and red symbols) concurrently computed as described in ref. [15]. The lines represent the corresponding exponential fit functions. The green dotes denote the Q_{ext} specification for C20 and C50 cavities, respectively, with $\Delta z_{FPC} \approx 31.8$ mm per design.

3.2 Input Coupler External Q Specification for C75 Cavities

In order to find the optimum Q_{ext}-value for the C75 cavities, a realistic assessment of the microphonic detuning level is required. Figure 15 shows the RF forward power (P_g) required for various values of the peak microphonic detuning (δf) up to 50 Hz as denoted and as a function of the Q_{ext}-value (colored lines). The black line corresponds to the optimum Q_{ext}, when P_g is minimal. Herein the characteristic impedance (R/Q) of the C75 cavity design as listed Table 3 has been used and a nominal field of E_{acc} = 19.07 MV/m assumed. At nominally L_{act} = 0.4916 m this yield an effective voltage (on-crest acceleration) of 9.375 MV. The maximum beam loading of I_b = 460 µA considered for the 12 GeV operation has been taken into account to cope with the power demands. The beam loading (P_b) is therefore 4.3 kW and represents the minimal power requirement at zero detuning. At a reasonably high unloaded Q (Q_0), the cavity RF losses play a minor role in this calculation. The Q_0-value has been set to 8e9, which results in 20.9 W dissipated in the cavity (P_c) at helium temperature (cf. section 5). The FPC coupling factor ($\beta = Q_0/Q_{ext}$) at zero detuning is then ≈207 given that in this case $Q_{ext} = Q_0/(1+P_b/P_c)$ = 3.86e7. Any microphonic detuning will yield a higher power requirement, while the optimum Q_{ext} shifts to lower values to minimize P_g.

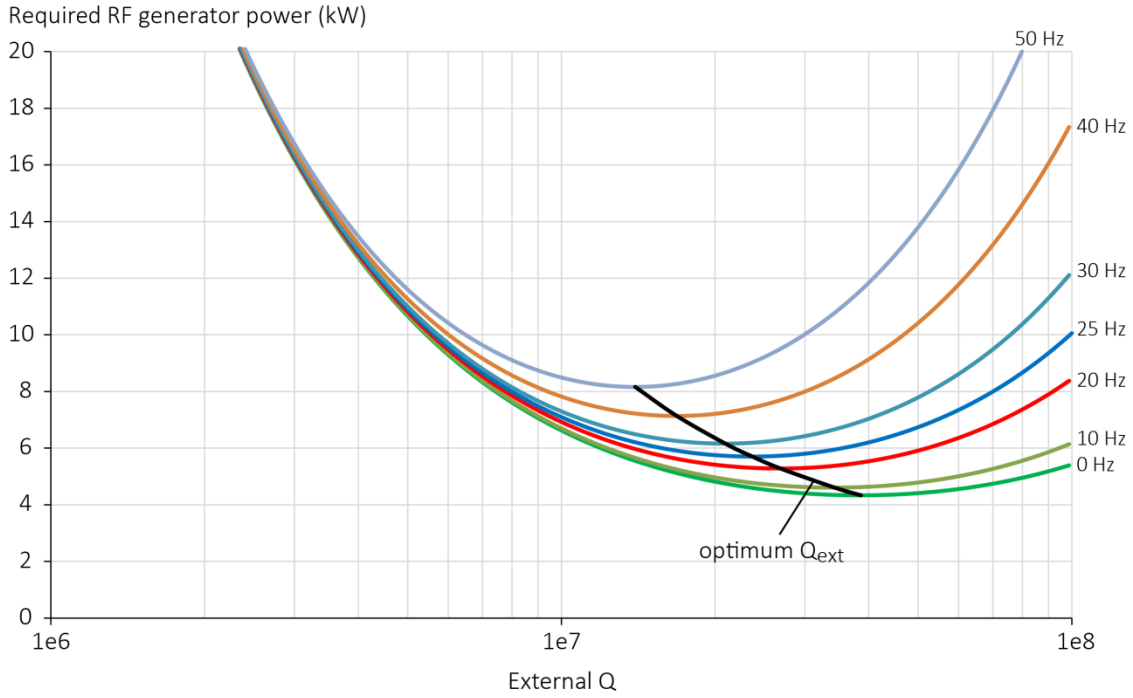

Figure 15: Forward RF generator power requirement for the C75 cavity as a function of the Q_{ext}-value at various speak microphonic detuning levels. The parameters used are: R/Q = 525.4 Ω, E_{acc} = 19.07 MV/m, L_{act} = 0.4916 m, I_b = 460 µA, and Q_0 = 8e9.

Table 6 lists the optimum Q_{ext}-values and the corresponding forward power requirements for the various detuning scenarios. With realistic microphonic levels, the requirement will exceed the specification of the C20 klystrons (5 kW). Therefore an upgrade of the RF system to 8 kW is conceived,

which requires the procurement of new 8 kW klystrons, high voltage power transformers, circulators, and electronics for the low level RF control systems. The 8 kW klystrons have the same footprint as the older 5 kW klystrons. The upgrade bears technically little risks since the RF system is identical to that already employed for a C100 upgrade cryomodule (R100) built at JLab and in operation in CEBAF's injector.

Table 6: RF forward power requirements for a C75 cavity at the optimum Q_{ext} in dependence of the peak microphonic detuning (E_{acc} = 19.07 MV/m or 75 MeV per CM energy gain)

Peak microphonic detuning δf Hz	Optimum Q_{ext}	Minimum P_g kW
0	3.86e7	4.33
10	3.43e7	4.60
20	2.69e7	5.28
25	2.37e7	5.70
30	2.10e7	6.16
35	1.87e7	6.64
40	1.68e7	7.13
50	1.40e7	8.16

Note that the RF incoming wave is attenuated along the waveguide (WR650) transmission line. For an estimated 50 ft. length, the loss for a typical WR650 waveguide (1100 Al alloy) is ≈0.1 dB at 1.5 GHz, the klystron circulator loss ≈0.3 dB and the waveguide filter loss ≈0.2 dB, yielding a total of 0.6 dB. This means that only ≈7 kW are usable to power the cavity. Moreover, the klystron should not be operated in saturation but in its linear regime. The peak microphonic detuning should therefore not be much higher than ≈35 Hz at E_{acc} =19.07 MV/m based on Table 6. This is realistically achievable. For instance, the following measurement data were reported for an original CM in CEBAF (Table 7) [16]. The average peak microphonic detuning is 13.7 Hz, while the maximum is 15.9 Hz. This may still not cover spontaneous microphonic excursions beyond this value, which can lead to cavity RF trips. Therefore six times the RMS value is accounted for as an allowance for the δf.

Table 7: Microphonic detuning as measured for cavities in an original CEBAF cryomodule (south linac zone 20 – SL20) [16]

Cavity Location	E_{acc} MV/m	RMS value (σ) Hz	6·RMS value (6σ) Hz	Peak Detuning Hz
1	3.8	4.1	24.7	15.1
2	4.8	3.1	18.7	10.0
3	6.8	2.8	17.0	15.9
4	8.0	3.8	22.9	13.7
5	3.3	3.8	22.7	14.6
6	8.3	3.6	21.4	15.4
7	4.0	3.5	21.1	14.0
8	5.9	2.3	13.6	11.0
Average value		3.4	20.3	13.7

The most recent microphonic measurements were performed for C50-13 as summarized in Table 8

[13], which includes the first C75 prototype cavity pair (C75-001 & C75-003). The averaged values are somewhat higher than those observed for SL20, with the 6σ = 25 Hz. For the C75 cavities a value close to but below 30 Hz has been achieved. A specification of δf = 30 Hz for the C75 cavities peak detuning allowance is therefore chosen.

Table 8: Microphonic detuning as measured for cavities in CM C50-13. Each of the values are the maximum values measured among several data sets (3-5) taken for each cavity

Cavity Location	Cavity SN	RMS value Hz	6·RMS value Hz	Peak detuning Hz
1	C75-001	4.7	28.2	11.9
2	C75-003	4.8	29.0	18.2
3	ia274	3.8	22.5	14.4
4	ia345	3.6	21.5	14.8
5	ia366	5.8	34.5	20.7
6	ia351	3.0	17.9	7.5
7	ia038	3.9	23.4	14.5
8	ia260	3.9	23.3	15.3
Average value		4.2	25.0	14.7

So far no contingency has been assumed for the energy gain. For C100 cavities a contingency of 7.5 % has been accounted for ($E_{acc,max}$ = 19.2 MV/m). This for instance allows other cavities to operate at a higher gradient to compensate for potentially lower-performing cavities not reaching the field specification. If we assume a similar contingency for C75 cavities, the design specification for E_{acc} raises to 20.5 MV/m (≈80.6 MeV per CM). Findings similar to Fig. 15 but for $E_{acc,max}$ = 20.5 MV/m are depicted in Fig. 16. The 7 kW line refers to the maximum forward power usable. At up to $\delta f \approx 31$ Hz the accelerating field can be sustained with 7 kW forward power, while Q_{ext} must be within 1.86-2.35e7 or, respectively, Q_{ext} = 2.1e7 ± 12 %.

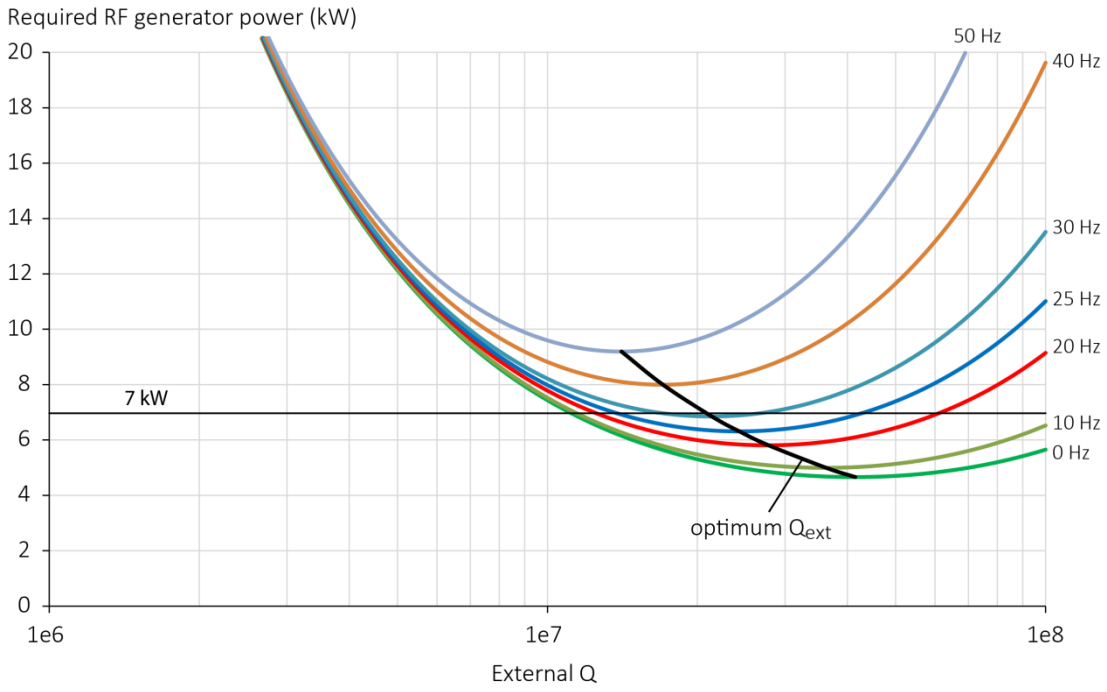

Figure 16: Forward RF generator power requirement for the C75 cavity as a function of the Q_{ext}-value at various speak microphonic detuning levels. The parameters used are: R/Q = 525.4 Ω, E_{acc} = 20.5 MV/m, L_{act} = 0.4916 m, I_b = 460 µA, and Q_0 = 8e9.

The allowable margin improves with smaller δf, but the optimum Q_{ext} shifts to higher values. Per calculation the separation distance Δz_{FPC} is 58.5 mm for Q_{ext} = 2.1e7. This is an increase of 26.8 mm compared to C20/C50 cavities. Given the detrimental impact to the damping of Higher Order Modes via the FPC (see following section) the separation between the FPC waveguide and the cavity should be constrained. As a reasonable compromise $\Delta z_{FPC} \approx 57.2$ mm has been chosen to result into exactly 1" (25.4 mm) added to the beam tube when compared to C20/C50 cavities. This equates to $Q_{ext} \approx$ 2e7 per design, which is not far below optimum value for the maximum allowable δf. In case a smaller δf is observed in the cryomodule, the Q_{ext} can be tuned readily upwards with the WR650 stub tuner since the increase is less than a factor of two. Even without tuning, the forward power required at Q_{ext} = 2e7 is not much elevated compared to the optimum value for δf = 20-40 Hz as shown in Fig. 16 and quantified in Table 9. Herein the absolute power requirements are listed for the optimum Q_{ext} in comparison to Q_{ext} = 2e7. The cases, which would not be supportable with the available generator power, are greyed out (δf > 31 Hz). The last column refers to a lower Q_{ext} = 1e7 as an example, which would not be supportable throughout, unless the WR650 stub tuner would raise the Q_{ext} again appropriately to allow for the case with δf < 31 Hz. A similar quantitative analysis for the nominal E_{acc} = 19.07 MV/m reveals that the maximum tolerable δf is 38.6 Hz with an optimum Q_{ext} = 1.73e7.

Table 9: RF forward power requirements for a C75 cavity at the optimum Q_{ext} and at Q_{ext} = 2e7 and Q_{ext} = 2e7 in dependence of the peak microphonic detuning (E_{acc} = 20.5 MV/m or 80.6 MeV per CM energy gain)

Peak microphonic detuning δf Hz	Optimum Q_{ext}	Minimum P_g at optimum Q_{ext} kW	Required P_g at Q_{ext} = 2e7 kW	Required P_g at Q_{ext} = 1e7 kW
0	4.24e7	4.66	5.31	7.44
10	3.69e7	4.99	5.48	7.53
20	2.81e7	5.81	6.00	7.79
25	2.45e7	6.31	6.39	7.98
30	2.15e7	6.85	6.86	8.22
31	2.10e7	6.96	6.97	8.27
35	1.90e7	7.41	7.42	8.50
40	1.71e7	8.00	8.07	8.82
50	1.41e7	9.19	9.62	9.60

Table 10 compares the findings for E_{acc} = 19.07 MV/m and E_{acc} = 20.5 MV/m. In conclusion, a Q_{ext} specification around 2e7 – by design – residing close to the lower end of the viable ranges for Q_{ext} as denoted for each case is conceived since the Q_{ext} can be raised readily by the stub tuner for all scenarios up to the tolerable δf given by the usable RF power of 7 kW provided by an 8 kW klystron. This Q_{ext} specification is set to regard for δf = 30 Hz, while potential higher microphonic detuning excursions are estimated to result in about one RF cavity trip per day. Moreover, a Q_{ext} = 2e7 limits the additional separation of the FPC to the cavity to 1" when compared to a C20/C50 cavity, which is compatible with the HOM damping requirements as shown in the following. As proven for C50 cavities, fabrication tolerances can be compensated by tuning the FPC body to achieve the toleranced margin.

Table 10: External Q range and peak microphonic detuning specification for a C75 cavity to support E_{acc} = 19.07 and E_{acc} = 20.5 MV/m with 7 kW usable forward power

E_{acc} MV/m	Max. tolerable δf Hz	Viable FPC Q_{ext} range	Q_{ext} specification
19.07	38.6	1.7e7 – 3.86e7	1.7-2.3e7 or 2e7 ± 15 %
20.5 (+7.5%)	31	2.1e7 – 4.24e7	

4. Higher Order Dipole Modes and Beam Break-up Impedance Threshold Analysis for C75 Cavities

The HOM damping in C75 cavities must suffice the CEBAF 12 GeV impedance threshold for multi-pass Beam Break-Up (BBU) instabilities, which is specified as 2.0e10 Ω/m for transverse deflecting modes [17]. This value shall not to be exceeded for dipole modes below the beam tube cutoff frequency. In this case full machine stability is guaranteed for all operating conditions satisfying 12 GeV baseline physics up to 100 μA injected beam current and with a margin for the injected beam current (200 μA) beyond any conditions contemplated by the physics division by 2009. A stricter specification of R_{tr} = 1.0e10 Ω/m discussed at the time would allow up to about 400 μA injected current, i.e. injected currents that are outside the original baseline design. In these specifications the dipole impedance $R_{tr} = R/Q_{tr}(r) \cdot Q_l$ at a given radial offset (r) from the beam axis is normalized by $k \cdot r^2$ with k being the wave number of the HOM. Higher order transverse modes usually play a minor role and are neglected.

As mentioned above, C20/C50/C75 cavities exhibit a comparatively large cell-to-cell coupling as well as only five instead of seven cells when compared to C100 cavities, which makes these less susceptible to trapped/confined HOMs. This is advantageous for strong HOM damping, while the achievable impedance eventually depends on the type and number of couplers [18]. Note that OC cavities by design have to rely heavily on the HOM damping through the FPC's rectangular waveguide, specifically for TE111 dipole modes, which resonate below the first cutoff frequency of the HOM waveguides ($f_{c,TE10}$ = 1.9 GHz). These cannot be damped by the HOM absorbers located at the far end of the HOM waveguides. While trapped below the beam tube dipole cutoff frequency ($f_{c,TE11}$ = 2.51 GHz), the damping of these HOMs can only be facilitated through the FPC waveguide instead ($f_{c,TE10}$ = 1.1 GHz). The dissipation of the HOM energy escaping through the FPC is realized with a broadband, small insertion loss (not greater than 0.2 dB per specification) waveguide HOM absorber/filter attached to each transmission line outside the CM as designed for C20 CMs. The filter is designed to minimize the attenuation of the incoming wave delivered by the klystron at 1497 MHz to satisfyingly low levels. Since the power dissipation is relatively low, the HOM filters do not need to be actively cooled.

Despite the strong cell-to-cell coupling, the broadband HOM damping efficiency in C75 cavities was verified numerically in 3D using the CST Design Studio code[6]. Since the FPC waveguide is placed further away from the end-cells than in a C20/C50 cavity, a less efficient damping of trapped dipole HOMs has to be taken into account because the evanescent fields leaking into the beam tube for these HOMs are now weaker when reaching the FPC endgroup. The damping also may depend on the mode polarization since the FPC is oriented in horizontal direction. Furthermore, the new cavity shape results in differing HOM frequencies and somewhat differing field pattern within the endgroups. The numerical findings are plotted in Fig. 17 by means of the dipole impedances covering the most critical HOMs. Herein a wakefield computation for the C75 cavity (green curve) is plotted as a guideline to identify crucial HOMs and their frequencies. The peak impedances are not all resolved yet, but via complex Eigenmode simulations (symbols) for both the C75 and C50 cavities.

[6] Numerical calculations prior to experimental measurement were necessary since the HOM damping of the trapped TE111 modes via the FPC can only be accurately determined when the FPC provides the same broadband damping condition as in a cryomodule, which is not feasible in a vertical test setup prior to cryomodule installation.

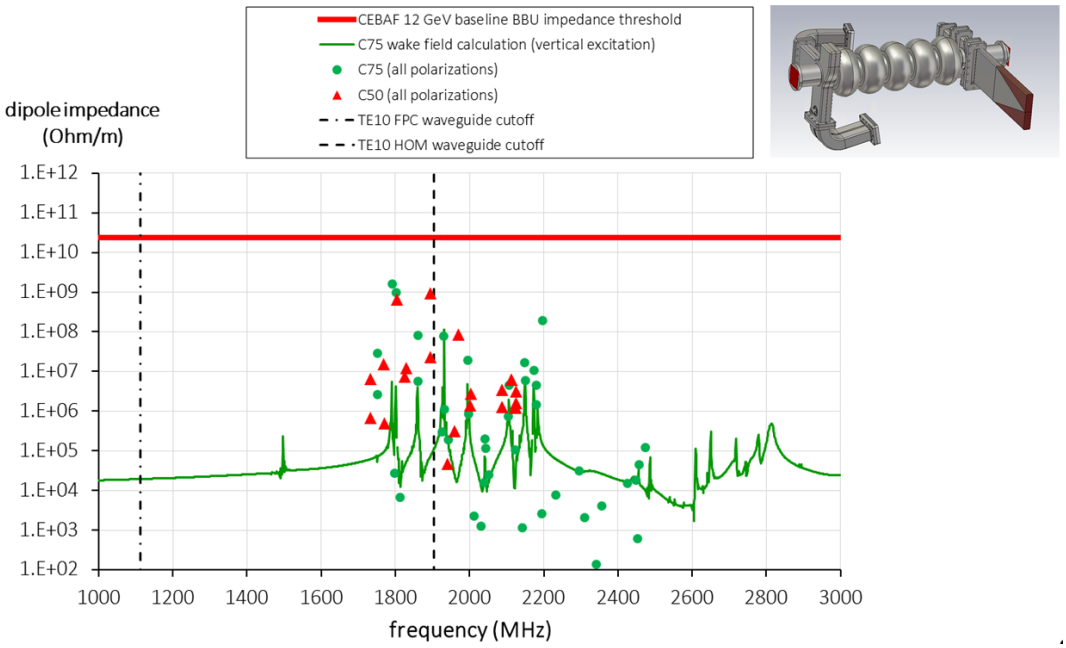

Figure 17: Dipole impedances as calculated for the C75 cavity (with FPC Q_{ext} = 2e7) and for the C20/C50 cavity as designed[7]. The horizontal line (red) corresponds to the multi-pass BBU impedance threshold specified for the CEBAF 12 GeV baseline physics.

In each case, the damping via the HOM waveguides has been accounted for by terminating the waveguide ends with models of the actual C20 absorber design assuming realistic frequency-dependent material properties, whereas the FPC waveguide (no dogleg) has been terminated with a broadband, dissipative load [15] as depicted in Fig. 17 (upper right). Note that no symmetry plane exists[8]. The red symbols refer to the findings for a standard C20/C50 cavity, the green dots for a C75 cavity with a Q_{ext} = 2e7 for the FPC. As in case of the C20/C50 cavity, all crucial dipole HOM impedances in the C75 cavities can be maintained below the 12 GeV baseline impedance threshold as well as below the stricter threshold of 1e10 Ω/m as described above. The highest dipole impedance in the C75 cavity corresponds to a TE111 mode around 1.8 GHz with maximally 1.6e9 Ω/m, which is about one order of magnitude below the allowable impedance threshold. Compared to a C20/C50 cavity, the maximum dipole

[7] The broadband impedance spectrum calculated for the C75 cavity (green curve) has been determined by a Fourier Transform of the wake potential excited by two 1D (line charge) Gaussian-shaped particle bunches (30 mm rms bunch length) traversing the cavity parallel to the beam axis on either side (two-beam excitation scheme) at the same distance (10 mm vertical offset each) and normalized by the bunch spectrum, while taking into account the combined bunch charge to evaluate the impedance amplitude. Since the C50/C70 cavity exhibits no symmetry plane, monopole modes are suppressed with this scheme, when one bunch charge has the opposite sign, while the excitation amplitude for dipole modes is doubled. The wakefield calculation had a finite length (142 m) and thus cannot resolve the peak impedances of high-Q HOMs. The impedance extrapolation scheme has been applied [19], which yet can only resolve the peak impedance values of those HOMs, for which the wake potential decays by a meaningful amount within the computed wake length. To verify full resolution of the HOMs, complex Eigenmode simulations (symbols) were performed providing both the R/Q and Qext values (equal to loaded Qs since no surface losses were regarded) of each HOM, the product of which results in the peak impedance values plotted.

[8] Due to symmetry-breaking effects caused by the HOM and FPC endgroup, the polarization of modes might not be purely horizontal or vertical. Therefore the Eigenmode results take into account the vector sum of the dipole impedances evaluated at a horizontal and vertical offset. Symmetry breaking is also responsible for the relatively large 'leakage' of the fundamental accelerating mode at 1.5 GHz in the broadband dipole impedance spectrum, since the wake potential of one particle bunch does not fully cancel that of the bunch with opposite charge traversing on the opposing side.

impedance is a factor of ≈2.5 higher, which is mainly caused by an increase in the Q-value of the specific HOM as a consequence of the larger axial separation of the FPC to the cavity.

5. Accelerating Field and Unloaded Quality Factor Specification

One of the main potentials of the refurbishment program is an improvement of the Q_0-value of the cavities by minimizing the RF power losses (P_c) per cavity dissipated into the Helium bath given by

$$P_c = \frac{(E_{acc} \cdot L_{acc})^2}{R/Q \cdot Q_0} = \frac{(E_{acc} \cdot L_{acc})^2}{R/Q \cdot G} \cdot R_S \quad (1)$$

Herein R_S denotes the average cavity surface resistance. This is particularly important since the required high field level in C75 cavities implies a much larger heat load for the cryogenic liquefier plant. Table 11 lists the nominal operational parameters and the resulting RF losses for C20, C50, and C100 cavities compared to a C75 cavity given the specified Q_0-values. For instance, the Q_0 specification for a C50 cavity is 6.8e9 at 2.07 K and E_{acc} = 12.5 MV/m corresponding to P_c = 12 W (≈95 W per CM). A C75 cavity at the same Q_0 would principally double the RF heat load at the nominal E_{acc} similar to C100 cavities. Maintaining the same losses however would require a Q_0 = 1.41e10, which is presently not achievable in CEBAF cryomodules (cf. section 7). As will be elucidated, a realistic target value of Q_0 = 8e9 at 2.07 K has therefore been specified for C75 cavities made from new material, which yields P_c = 20.9 W[9] per cavity nominally (≈167 W per CM). The additional heat load from a C75 CM compared to a C50 CM is deemed acceptable in consideration of the capacity of the central helium liquefier plant.

Note that the RF heat load arising from the cavities is about 22% lower for a C75 CM than for a C50 CM at any given energy gain (i.e. P_c = 9.3 W, ≈74.3 W per CM at 50 MeV) as a consequence of the new cell shape and the prospected Q_0 improvement.

Table 11: Nominal operational parameters of JLab cavities and resulting RF heat loads dissipated in the helium bath

Cavity type	Cell shape	Energy gain per CM	E_{acc}	B_{pk}	Q_0 at 2.07 K	P_c	P_c per CM
Units		MeV	MV/m	mT	MV/m	W	W
C20	OC	20	5	22.8	2.4e9	5.4	43.1
C50	OC	50	12.5	57.0	6.8e9	11.9	95.2
		50	12.5	57.0	4.6e9 (average Q_0)	17.7	141.6
C100	LL	100	17.86	66.8	7.2e9	25.7	205.5
		107.5	19.2[a]	71.8	7.2e9	28.9	231.0[b]
C75	HC	75	19.07	79.7	8e9	20.9	167.3
		80.6	20.5[a]	85.7	8e9	24.2	193.3[b]
		50	12.7	53.1	8e9	9.3	74.3
		75	19.07	79.7	6.8e9 (C50 Q_0)	24.6	196.8
		75	19.07	79.7	1.41e10 (C50 P_{RF})	11.9	95.2

[a] Specification with 7.5% contingency for energy gain

[b] Below CM capacity limit specification of 250 W

Yet, the specified Q_0-value for refurbished C50 cavities has never been met, which raised the

[9] This is safely (more than one order of magnitude) below the total heat capacity of a cavity [20],

question of whether the C75 cavities can meet the even higher specification. Figure 18 depicts the measured Q_0-values (at or close to 2.07 K) of the refurbished cavities during the CM commissioning in the CEBAF tunnel at E_{acc} = 12.5 MV/m or alternatively at a lower field level when cavities were performance-limited. The average Q_0-value is 4.4e9 (black line). This is ≈1/3 below the specified value. There is no obvious correlation identifiable between the cavity position and the Q_0-value.

The important result is that two C75 prototype cavities (highlighted) built at JLab and installed in C50-13 in 2017 have achieved the highest Q_0-values among all refurbished cavities. One cavity met the new specification (Q_0 =8e9), the other is only slightly below (Q_0 =7.5e9). The C75 cavities are the first cavities installed in CEBAF produced from ingot material with the prospect of maintaining a higher Q_0-value.

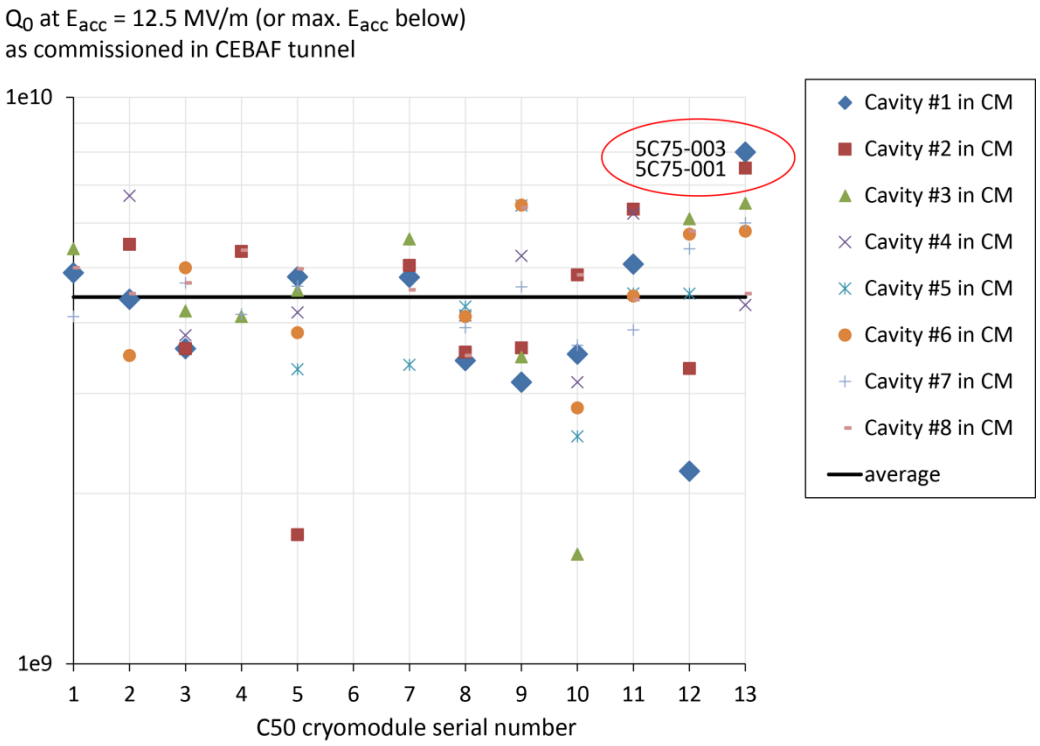

Figure 18: Q_0-values around 2.07 K at E_{acc} = 12.5 MV/m – or alternatively the maximum field achievable below E_{acc} = 12.5 MV/m – of refurbished C20 cavities as measured during commissioning of the cryomodules in the CEBAF tunnels. No data are available for C50-06 due to a leaky JT-valve. Cavity position #1 is close to the helium supply end can and cavity position #8 is close to the helium return end can. These cavities are closest to the warm optical beam line girders that interconnect adjacent cryomodules.

6. Prospects of (Medium-Purity) Large Grain Ingot Material

To target an as high as possible Q_0 achievable for C75 cavities in the cryomodule, it has been decided to utilize large grain (*LG*) discs cut from ingot Nb material instead of fine grain (*FG*) sheets for the cells of the HC cavity. In fact, *LG* material has been proven to yield similar or better performance than cavities made from *FG* material with the same purity – per residual resistivity ratio (*RRR*) – and after standard surface post-processing treatments (e.g. [21]). Standard processes include BCP, EP, high temperature vacuum furnace annealing, and low-temperate baking. R&D conducted at JLab for 1.3-1.5 GHz single-cell cavities made from medium ($RRR = 100 - 200$) and low-purity ingot Nb ($RRR = 60$) and RF tested in JLab's vertical test area (VTA) concluded that cavities with medium-purity ($RRR \approx 120$-150) exhibit an average quench field of $B_{pk} \approx 100$ mT [22] (though high-purity ingot cavities ($RRR > 250$) more readily achieve higher field levels of ≈120 mT on average [23]). This would equate to $E_{acc} = 23.9$ MV/m for a C75 cavity made from the same material. Moreover, an average Q_0-value of 2e10 at 2 K has been obtained at $B_{pk} = 70$ mT (equates to $E_{acc} = 16.7$ MV/m for a C75 cavity) for cavities made from medium-purity ingot Nb resonating after BCP or EP thanks to a reduced BCS resistance (R_{BCS}) and residual resistance (R_{res}) of *LG* compared to high-purity *FG* material. The cost of medium-purity ingot Nb discs is about a factor of three lower than that of *FG* sheets. Another advantage of medium-purity material is a ≈20% lower R_{BCS} as a result of a smaller mean free path of the normal electrons [23]. The residual resistance is low as well (~2nΩ) [24], and the field dependence of the Q_0-value is weaker than in *FG* cavities with the average surface resistance at low fields being maintained up to ≈20 MV/m The findings from vertical RF tests are summarized in Fig. 19. An additional advantage of ingot Nb material is that it has much better ability to expel residual magnetic field during cool-down across T_c, which is very important for a cryomodule design such as the original CEBAF one in which it was proven to be difficult to maintain a low residual magnetic field. Motivated by this perspective, three prototype HC cavities have been manufactured recently from Nb ingot as part of a C75 R&D program.

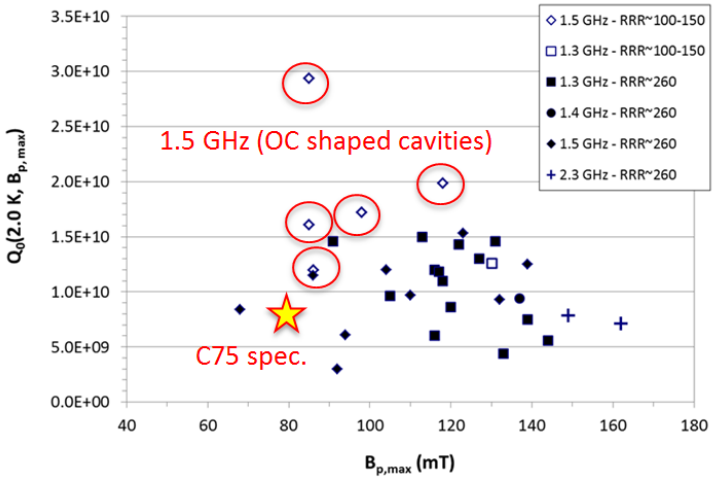

Figure 19: Distribution of quality factors at 2 K just below the quench field limit (over 30 single- and multi-cell cavities) as a function of quench fields for cavities made from CBMM ingot material of different purity. The findings for *LG* cavities with OC shape are highlighted (red circles) and exceed the specification (star symbol) for the C75 cavity. Results are taken from ref. [1].

6.1 C75 Large Grain Prototype Cavity Experience and Test Results

The experience with the fabrication, processing and production of the first three C75 prototype *LG* cavities is described in [25]. The main issue affecting the cavities quench field was related to defects in the equatorial electron beam welds. The EBW machine encountered several different failure modes throughout the year. E.g., a damaged (vendor obsolete) electronic board required for controlling an electron beam steering coil had to be replaced, while burned-up cables were found. Later, a bearing wheel for a steering coil (Y direction) was mechanically gridlocked after several years of operation and had to be replaced not long after the C75 cavity fabrication. This could have been an issue for previous electron beam control. Most recently the voltage on an Opto-22 isolator board was lower than the 5.0 VDC specified and the power supply was adjusted, which consequently raised the current and burned out an on-board fuse, which had to be replaced. The EBW machine has since been serviced and electronics upgraded. Issues with the camera system still persist, making the alignment of inside/outside welds difficult.

In order to avoid issues with electron beam welding, which is crucial to achieve high accelerating gradient, it is preferable to have future production C75 cavities built by a qualified, experienced company with state-of-the-art EBW facility.

Figure 20 shows the results from the RF test of cavities 5C75-001 (made from medium-purity ingot Nb) and 5C75-003 (made from high-purity ingot Nb) in the vertical cryostat and in the cryomodule. The data show that there was no significant change in performance. The biggest difference is the reduction of Q_0 by ≈40% between the test as a single-cavity and as part of the cavity pair, in the vertical cryostat. When tested in the cavity pair configuration, the Nb dogleg housing the cold RF ceramic vacuum window is installed to each cavity FPC waveguide port as well as the HOM waveguide elbows with HOM absorbers. Similar reduction in Q_0-value had also been measured in an OC cavity (IA366) after the dogleg, RF window and top-hat had been installed. This implies that additional RF losses arise in the FPC waveguide. RF losses leaking into the 2K helium bath can arise from the normal-conducting metallization around the window, which is required for the braze joint of the ceramic to a Nb eyelet. Yet, the Q_0-value of 5C75-003 did not degrade, though already smaller than for 5C75-001. Additional investigations therefore required to understand the loss mechanisms in C20 CMs not directly related to the cavity. Furthermore, the Q_0 typically degrades significantly after cavities are installed in the cryomodule, which can results from high residual magnetic fields causing an increase of the cavity surface resistance. Possible sources for the Q_0 degradation are discussed in the following sections.

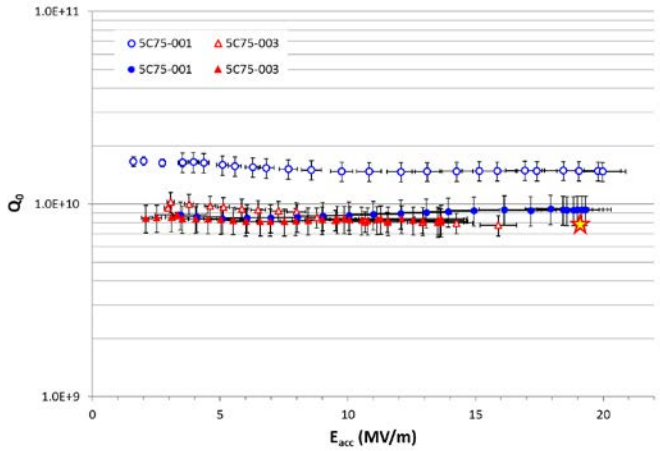

Figure 20: VTA results at 2.07 K for 5C75-001 and 5C75-003 (left) before (empty symbols) and after (solid symbols) assembly into a cavity-pair [25] and $Q_0(E_{acc})$ scaled to 2.07 K measured during cryomodule commissioning (right). **We will add a $Q(E_{acc})$ plot from Mike with error bars.**

7. Q_0-Degradation in Cryomodules and Countermeasures

7.1 Magnetic Hygiene

C50 cavities with typical Q_0-values in the lower 1e10 range in the operating regime as measured in vertical tests do not meet the Q_0 specification once installed in the cryomodule. The average Q_0(2.07 K) determined during cryomodule commissioning is 4.4e9 based on Fig. 18 shown further above, thus about a factor two degradation, which is also true at low operating fields. In contrast, the performance specifications (Q_0 and E_{acc}) for upgrade cavities installed in ten C100 CMs built between 2010 and 2014 were dominantly met both in the VTA and during cryomodule commissioning. The main Q_0-degradation in original CMs is therefore assumed to be caused by an increase of the residual surface resistance due to trapped magnetic flux either from remanent fields of magnetized cryomodule and cavity components or from magnetic fields generated by thermocurrents. These effects are not pronounced in updated C100 CMs, which utilize improved magnetic shields and less magnetizable materials. Also, the mechanical tuner is installed outside the helium vessel, which surrounds each cavity closely. In 2008 it has been suspected that the original shielding of the Earth magnetic field (≈0.5 Gauss) in C20 CMs is insufficient. Note that C20/C50 cryomodules have an outer shield made from high permeability magnetic sheet material located below the first superinsulation of the cryomodule vessel and an inner magnetic shield wrapped around the cylindrical stainless steel (SS) helium vessel. At this time a magnetic field survey at room temperature probing into the beam pipe revealed poor shielding, particularly for the axial component with a shielding factor as low as 1.6, while the transverse shielding factor was estimated to be on the order of 30 [27]. Moreover, all shielding materials suffered from a drop of the permittivity when cooled down to cryogenic temperature and are since replaced. The more suitable Cryoperm alloy material, which is known to perform well at cryogenic temperatures, has been implemented for the inner shield (≈0.5 mm thick, factor ≈1.4 thicker than old shield), while for the outer shield Amumetal (≈1 mm thick, factor 4 thicker than before) has been chosen. The saturation limit,

above which the magnetic shielding can reduce drastically, is 8 kG for Amumetal and 9 kG for Cryoperm. The calculated shielding factor for the axial field was between 85 and 116 with the new shielding design [27]. Yet, magnetizable components of the cold mechanical tuner assembly still reside within SS helium vessel. Already by 2007, the tuner ball screw in close vicinity of the cavity surface has been identified as a possible culprit to possess a high remanent magnetic field, however its impact on the cavity Q_0 was shown to be negligible during vertical tests. Nevertheless, a shielding box was developed and employed from CM C50-06 onward but discontinued for C50-12 and C50-13, since no significant difference in cryomodule cavity performance was found.

Work conducted in 2014 on components for CM C50-11 had verified that the tuner rods, strut springs, ball bearings and ball screw blocks tend to have a relative permeability >6 and a residual magnetic field. Moreover, the tuner strut-spring material has been replaced with stainless steel 316 L and the ball screw shielding box further improved starting with CM C50-11 (for then four cavities), which yielded some Q_0-improvement (compared to the other four cavities in the same CM) as measured in the CEBAF tunnel, though still a Q_0 of only around 6e9 could be reached [28].

A recent survey of the remanent field of the helium vessel as removed from CM FEL02 exhibited fields up to ≈700 mG on contact at the location of the instrumentation port and ≈100 mG on contact at places where welds had been ground. Such fields result in regions with ≈10 mG above background at the cavity equators [29]. Furthermore, a systematic study as part of a magnetic 'hygiene' effort has been conducted with a C20 cavity (IA366, meanwhile installed in C50 CM-12), which then only received a high pressure rinse after the CM disassembly [29]. VTA tests were done with and without tuner, with and without He vessel and inner magnetic shield. The tests were also done with different residual magnetic fields and cool-down rates. The only condition which resulted in a Q_0-value comparable to that measured in a cryomodule was when the cavity was cooled in the presence of a residual field of ~50 mG. The possible origin of such high magnetic field close to the cavity remained unclear [29].

In order to "protect" as much as possible the cavity from any residual magnetic field, it was proposed to install a magnetic shield as close as possible to the cavity itself. The shield, shiwn in Fig. 21, was designed to achieved a shielding factor of ≈10, which should result in a residual field of < 10 mG at the cavity surface once the outer and inner cryounit's magnetic shield are installed. It was verified experimentally with a prototype shield that such low residual field could be achieved.

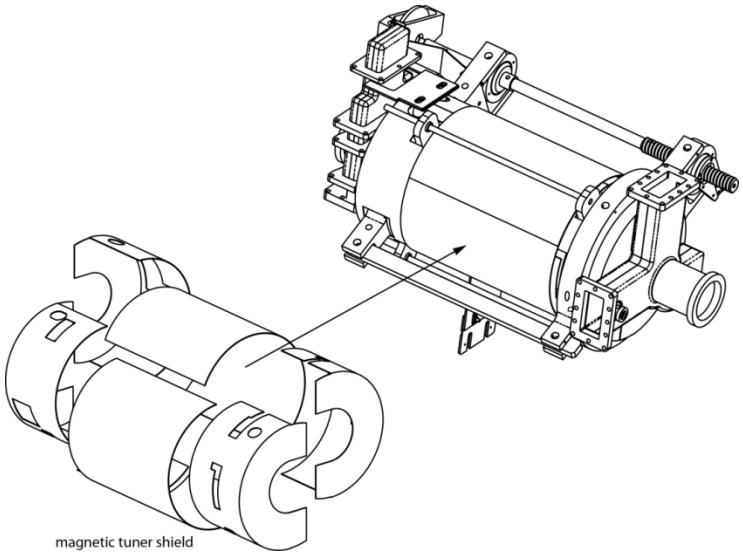

Figure 21: C50/C75 cavity magnetic shield design assembly which will be located inside the stainless steel helium vessel of a cavity pair [28]. The shield is made from Cryoperm material, which shall provide a higher permeability at cryogenic temperature than at room temperature. The cavity magnetic shield has first been employed in CM-013 for all cavities.

7.2 Low-Temperature RF Windows Losses

The FPC waveguide houses a room temperature RF window just outside the cryomodule and a low-temperature (2 K) RF window, which resides at the helium vessel interface. Any RF losses in the cold window can thus be readily transferred to the helium bath. The space between the windows is evacuated to provide an insulation vacuum using an ion pump. The waveguide insulation vacuum was conceived originally as a precaution in case metal from the interior waveguide surfaces would RF sputter onto windows and thus metallize the surface causing overheating, which in turn could fracture windows and contaminate the cavity vacuum with air-borne particulates and ceramic fragments. For C20/C50 cavities a single pump is used to evacuate both waveguides of a cavity pair, while for C75 cavities it is foreseen to equip each waveguide with a vacuum pump. The cold window is welded into the outer flange of the dogleg. The cold C20 RF windows are recycled for refurbished cavities if they pass a low power acceptance test in the VTA at 2 K (see further below). To minimize dielectric losses ($\pi \cdot f \cdot \varepsilon_r \cdot tan\delta \cdot Int(dV \cdot |E|^2)$), wherein ε_r denotes the relative permittivity and $tan\delta$ the loss tangent, the ceramic is made from high-purity poly-crystalline alumina (Al995, 99.5% Al_2O_3, ε_r within 9-10). There could be only limited data found in published literature concerning the loss tangent at L-band frequencies and at 2 K, but measurements suggest that the $tan\delta$ reduces from the lower 10^{-4} range at room temperature [30] to within 10^{-6} and 10^{-7} at liquid helium temperatures [31].

The ceramic is brazed into a Nb 'eyelet', which will be superconducting during operation to minimize RF losses. The Nb eyelet itself is eventually dropped into the upper flange of the dogleg, where it is EB welded to the flange. The eyelet is rather thin (≈250 µm) and thus flexible, which minimizes structural stresses at the ceramic-to-metal interface, which is proven to withstand thermal cycling. A portion of

the upper dogleg flange housing the Nb eyelet and ceramic window is depicted in Fig. 29 together with a photo of a used ceramic assembly with view onto the bottom.

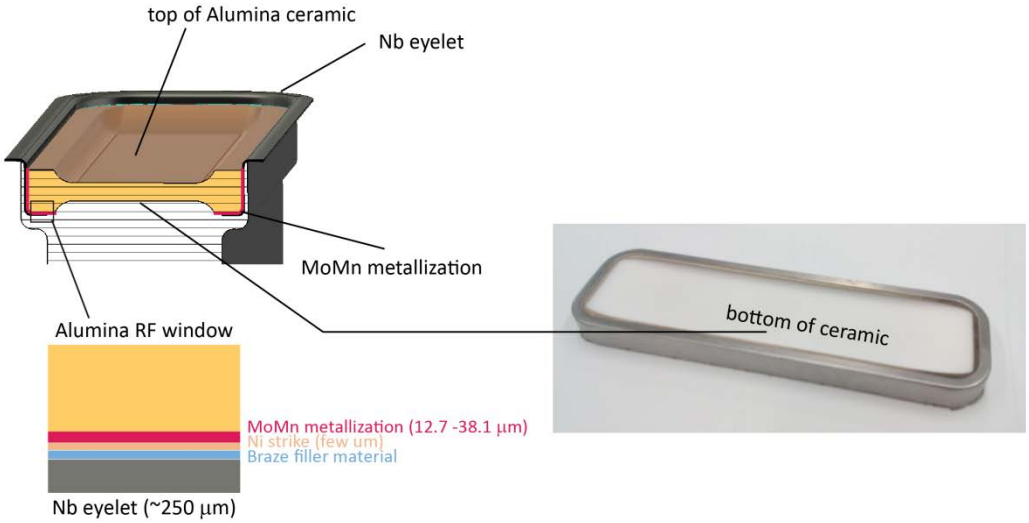

Figure 29: Illustration (top left) and photo (right) of a standard cold RF ceramic windows as brazed to a Nb eyelet. The brazing scheme of the ceramic to the Nb is shown at the bottom left.

To braze the ceramic to the Nb eyelet with a strong bond, it needs to be metallized first. The metallization is done on the perimeter of the ceramic and to some extent around the perimeter at the bottom (see photo in Fig. 29), where it is still surrounded by the eyelet. The brazing utilizes the common molybdenum-manganese/nickel plating method. Hereby the ceramic is coated first with molybdenum and manganese particles (12.7-38.1 µm thick usually mixed with glass additives) and the coated ceramic is then fired in a reducing wet hydrogen atmosphere (typically at 1450-1600°C). The fired coating is followed by a nickel plating/strike, which is then sintered (typically at 850-950°C) in a dry hydrogen environment. The Ni plating improves the wettability for a standard braze filler metal (foil) utilized to eventually braze the ceramic to the Nb eyelet in a vacuum furnace. Capillary forces will results in a uniform braze filling the gaps at the sides and bottom of the ceramic within the Nb eyelet for a UHV-tight seal.

While the Nb eyelet shall be superconducting during operation, the metallization as 'seen' by the RF is normal conductive (NC). The Mo-Mn metallization is thick enough for the RF fields to strongly decay and dissipate in the NC coating before reaching the Ni plating (RF skin depth is sub-µm to a few µm at 1.5 GHz and depending on the actual conductivity (σ) at cryogenic temperature). Molybdenum has a conductivity of σ(20°C) ≈1.9e7 S/m, which improve to 4.9 S/m at 1.5 K [32]. Manganese is a poor conductor with σ(20°C) = 6.9e5. The conductivity of the Mo-Mn metallization layer at the operating temperature is unknown, but it is assumed not be better than for the pure Mo.

To allow an estimation of the metallization losses only, i.e. fully isolated from any other potential loss source, numerical calculations have been done for a C20/C50 cavity including the dogleg and RF window assembly followed by a straight section of the FPC. This is identical to the model used for Q_{ext}-simulations described before. This time however the portion of the ceramic, where the window is metallized, has been modelled as a thin NC metal layer.

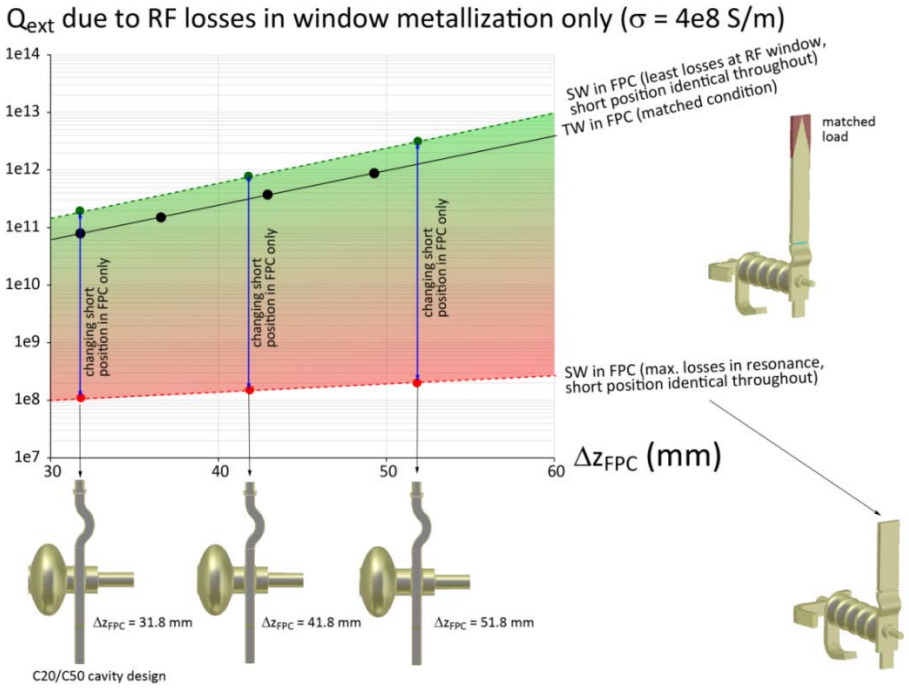

Figure 30: External Q as a consequence of normal-conducting RF losses in the window ceramic metallization (Q_{ext_window}) for a C20/C50 cavity in dependence of the distance between the center FPC waveguide center and the end-cell iris (Δz_{FPC}). Refer to text for further explanations.

Dielectric (volumetric) losses in the window were disregarded for simplicity though these will add to the losses depending on the loss tangent (but found to be a much smaller fraction of the total losses when loss tangent was 1e-6). The cavity Nb surface and any other surfaces have been set as perfect electric conductors (PEC). Given the stored energy in the cavity (W_s), an external Q due to the metallization losses is derived (Q_{ext_window}), which is used to estimate the potential Q degradation in a cavity. This is depicted in Fig. 30. A conductivity of σ=4e8 S/m has been assumed for the Mo-Mn metallization layer, which still could be rather optimistic considering the presence of Mn. The RF losses and thus Q_{ext_window}-values can be readily scaled to any other conductivity value (square root dependency). The nominal separation Δz_{FPC} for C20/C50 cavities is 31.8 mm as already discussed previously. In the simulations, 10 mm and 20 mm have been added (horizontal axis), which will increase the external Q of the FPC. Increasing the external Q implies that the external power in the waveguide (P_{ext}) is reduced according to $\omega \cdot W_s = Q_0 \cdot P_{cav} = Q_{ext} \cdot P_{ext}$, while the Q_{ext} of the FPC follows the usual exponential dependency as a function of Δz_{FPC}. As indicated by the vertical (blue) arrows, the Q_{ext_window} may vary by more than four orders of magnitude between the extreme limits. This implies that losses depend sensitively on the boundary condition set at the end of the FPC waveguide. When a closed boundary is simulated it will create a reflection plane and thus a standing wave (*SW*) condition. Either a *PEC* or perfect magnetic boundary (*PMC*) can be applied, which provides a *SW* separated by a quarter of the RF guide length ($\lambda_g \approx 0.3$ m at 1.5 GHz, while $\lambda_{cutoff} \approx 0.27$ m). The two corresponding solutions principally enclose all other solutions, which in turn can be found by changing the position of the reflection plane within $¼\lambda_g$. The RF losses could be increased in dependence of the waveguide length for a *PEC* boundary to peak resonantly at a certain length, which did alter when changing Δz_{FPC}. A

corresponding model is illustrated in Fig. 31 (Δz_{FPC} = 31.8 mm).

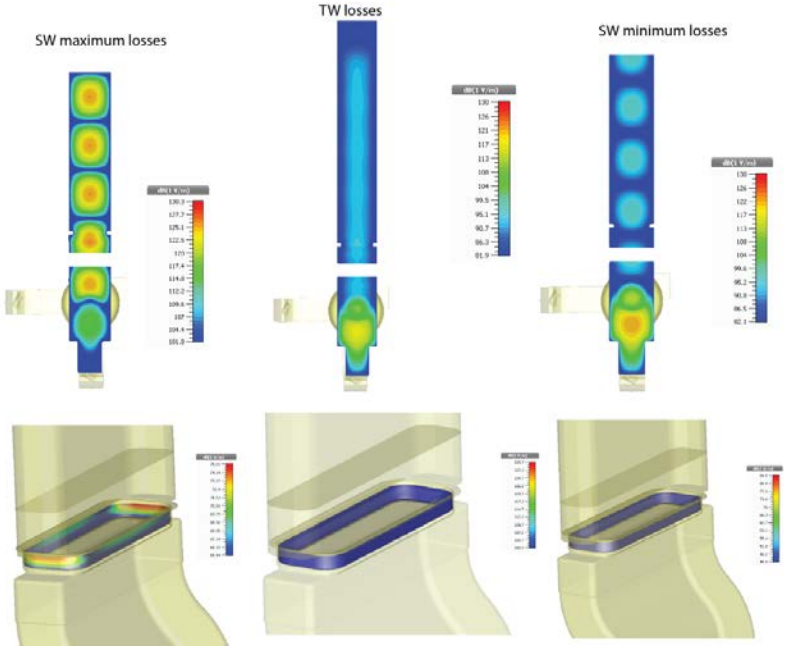

Figure 31: Electrical field contours (top row, side view of cavity) in the center of the FPC waveguide for varying boundary conditions (left: SW with PEC boundary, mid: matched load with time averaged TW, right: SW with PMC boundary). The bottom row shows the corresponding magnetic field contours around the RF window metallization simulated as a thin metal. Strongest/weakest RF fields are colored red/dark blue.

The top row depicts the electric field contour in the center of the FPC waveguide (side view of cavity) for three different boundary conditions (W_s = 1 Joule throughout). For the *PEC* boundary condition (left) the RF losses in the metallization are maximized. Q_{ext_window} then drops drastically to the lowest value. The RF magnetic field contours around the metallization are shown in the bottom row of Fig. 31, which reveals that the peak RF currents occur on the short of side of the eyelet (red color).

For the same model Q_{ext_window} is maximized, when changing the reflection plane condition from PEC to PMC (right), i.e. RF losses at the metallization are now minimal (dark blue color of magnetic field contours). With a matched boundary condition on the other hand, a TW is created. The time-averaged RF fields are depicted in the mid of Fig. 31. The resulting average RF losses are rather low and much less than for the worst SW scenario. The corresponding Q_{ext_window}-values follow the black line in Fig. 30. By increasing the separation Δz_{FPC}, the Q_{ext}-value of the FPC increases, which concurrently mitigates the RF losses at the window metallization for the same FPC length and boundary condition. A larger separation of the FPC waveguide to the cavity is therefore favorable by design. This has been conceived for the C75 cavities as already discussed in section 3 to optimize the generator power requirements based on the microphonic detuning allowance and in consideration of HOM damping requirements.

For a cavity fed by an input coupler at frequency f in absence of beam loading – as during CM commissioning – a large fraction of the incoming generator power is reflected since the FPC is strongly over-coupled ($\beta = Q_0/Q_{ext} \gg 1$). The portion of the power into the waveguide is given by:

$$P_c(f) = \frac{4 \cdot P_g}{Q_{ext} \cdot Q_0} \cdot \frac{1}{\left(\frac{1}{Q_{ext}} + \frac{1}{Q_0}\right)^2} \cdot \frac{1}{\left(\frac{f}{f_0} + \frac{f_0}{f}\right)^2} \qquad (2)$$

For an Eigenmode solution we have $f = f_0$ and since $Q_0 >> Q_{ext}$ we find

$$P_c(f_0) \approx 4 \cdot P_g \cdot \frac{Q_{ext}}{Q_0} \tag{3}$$

In practice one has to take into account that waveguide reflections due to impedance mismatches may occur along the input power transmission line up to the klystron circulator load, e.g. within waveguide tapers, bends, at flanges and other discontinuities. Also during beam operation a residual reflection of the incoming wave remains when trying to minimize the reflected power under a certain beam loading condition. As detailed above, the CEBAF WR650 stub tuners are used to minimize the required input power by optimizing the Q_{ext}-value via a resonant low-Q coupling circuit for an otherwise fixed Q_{ext} of the FPC. As with a closed boundary condition, the stub tuner plungers – when inserted in the waveguide – will create a *SW* component between the cavity coupling iris and the plungers that will allow a Q_{ext} adjustment. The RF fields downstream at the cold RF window are therefore altered depending on the actual tuning. This can create differing, yet unknown loss scenarios, particularly since plunger settings may change from cavity to cavity as transmission line lengths are not necessarily identical. To study such scenarios numerically, a simple stub tuner with three plungers (separated by ¼ λ_g) has been modelled. The plungers were positioned between the RF window and a matched load (e.g. resembling the circulator load). To limit the model to a reasonable size, only a short section of the FPC beyond the dogleg and window has been allowed for[10]. With a narrow waveguide wall of about 1" in this section, the plungers were inserted up to 0.9" into the waveguide (referred to as 'fully' inserted). The findings are shown in Fig. 32, which plots Q_{ext_window} (no further RF losses) versus the external Q of the FPC determined by the external losses in the matched load.

[10] In the CEBAF tunnel this section would be located before the first vertical waveguide bend, which is followed by a tapered transition to the WR650 waveguide size, although the warm window has not been included in the simulation for simplicity.

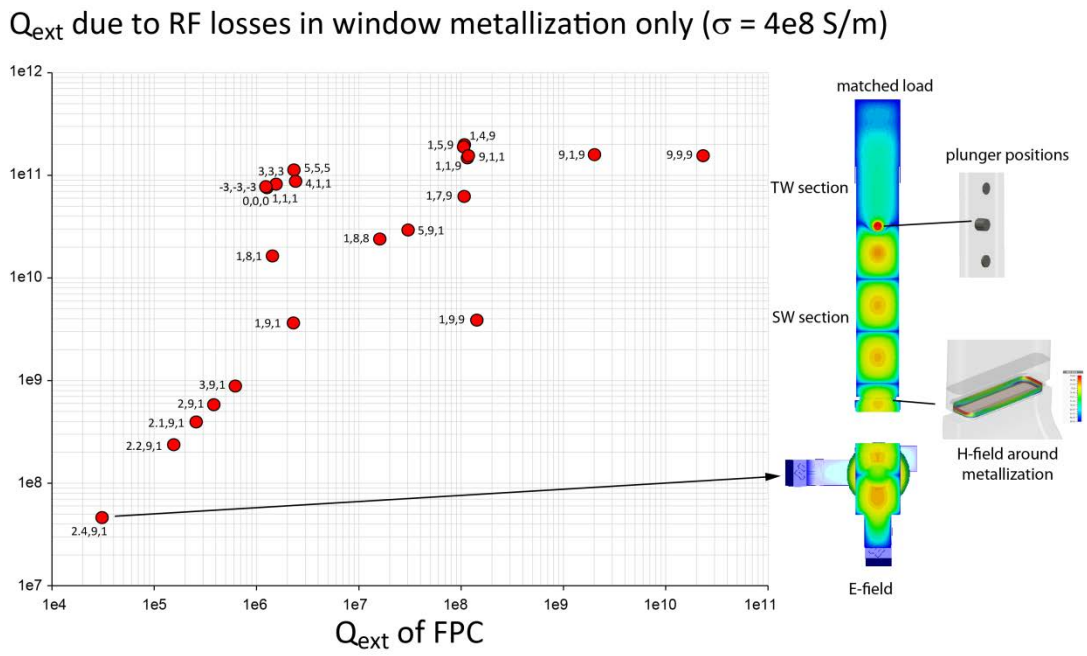

Figure 32: External Q of a C20/C50 cavity (Δz_{FPC} = 31.8 mm) numerically computed as a consequence of normal-conducting RF losses in the window ceramic metallization in dependence of the external Q of the FPC tuned to various values by a three-stub tuner position between the dogleg and a matched load at the end of the FPC waveguide (cf. figures to the rights). Note that in one case the plungers were all retracted (-3,-3,-3) leaving some vacuum volume outside the broad wall, which resulted in only a slightly lower external Q of the FPC compared to the setting when all plungers were flush with the wall (0, 0, 0). See text for further explanations.

Again a conductivity of σ = 4e8 S/m has been assumed for the Mo-Mn metallization to be consistent with the calculations above. This could still be an overestimation such that the actual Q_{ext_window}-values would shift down vertically. To differentiate among the varying plunger positions, the number triplet (X, Y, Z) is utilized to denote each plunger position in 1/10" starting with the first plunger closest to the cavity. The setting (0, 0, 0) refers to all plungers being flush with the waveguide wall. Fig. 32 in fact reveals that RF metallization losses cover close to four orders of a magnitude for the limited plunger settings computed. This is comparable to the findings in Fig. 30, where a reflection plane has been used. An FPC's Q_{ext}-value of 1.24e6 has been achieved with the plungers at (0, 0, 0), which agrees with the earlier calculation (see Fig. 15). With at least one plunger fully inserted, the Q_{ext}-value of the FPC can be readily tuned up, eventually by more than four order of magnitudes to 2.3e10 when all plungers were fully inserted (9, 9, 9). The RF metallization losses in this case are comparably small. In contrary, the Q_{ext}-value of the FPC could be minimized by a factor of ≈40 – when referred to (0, 0, 0) – down to 3.1e4 at setting (2.4, 9, 9). When the 1st plunger was further inserted, the Q_{ext} of the FPC increased again. The variation of the FPC's Q_{ext}-value hence covers almost six orders of magnitude. A full insertion of the 2nd plunger inside the waveguide has been important to lower the FPC's Q_{ext}. At the lowest Q_{ext} of the FPC, the Q_{ext_window} dropped drastically into the 1e7 range. In combination with the 1st plunger it could be reduced from 2.3e6 (1, 9, 1) to the mentioned 3.1e4, while Q_{ext_window} decreased linearly at the same time from 3.6e9 to 4.6e7. The RF losses increased by a factor ≈80 according to $\omega \cdot W_S / Q_{ext\_window}$ within

this range and thus with a single plunger change of merely 0.14". Such a 'catastrophic' scenario might be similar to that reported in CEBAF, i.e. when stub tuning of Q_{ext} down – by only a factor of two – consistently yields excessive window heating.

In general, when lowering the FPC's Q_{ext}-value, the out-coupled power is increased in the TW section, while the SW between the stub tuner and cavity yields elevated fields compared to those in the TW section, which inevitably yields higher RF losses in the window. The electric field contour corresponding yielding the maximum RF losses is depicted on the right of Fig. 32 together with magnetic field contours around the metallization. Both plots closely resemble the RF field pattern in Fig. 31 resulting in the highest RF losses, except that there is a traveling wave component beyond the stub tuner towards the matched load. The numerical simulations validate that the plunger positions can sensitively alter the SW conditions and significantly influence the RF power dissipation in the cold window. This can burden the heat load for the cryogenic system and can lead to a Q-degradation according to $(1/Q_0 + 1/Q_{ext\_window})^{-1}$, wherein Q_0 is the unloaded Q associated with the cavity surface only.

As discussed above, the conductivity of the window metallization and the dielectric losses of the alumina ceramic are not accurately known at 2 K, but a quality control of C50 cold RF windows has been implemented since 2008 (first for C50-07) to quantify the RF losses of each window individually. For this reason a low power 'double-dogleg' setup has been conceived as depicted in Fig. 33 joining two Nb dogleg/window assemblies with a straight Nb waveguide. Furthermore, two Nb waveguide-to-coax adapters are used, one on each end to allow transmission measurements via a Vector Network Analyzer (VNA), when the RF structure is fully immersed in helium and cooled down to 2 K in a vertical Dewar. The setup is symmetric with respect to the center plane.

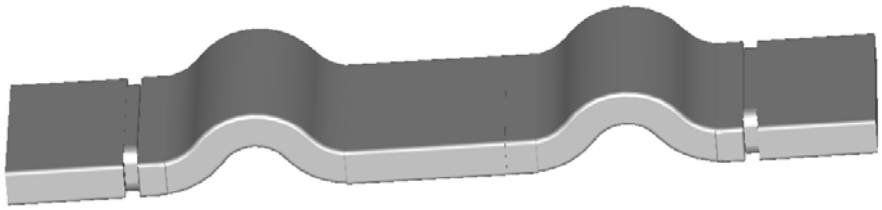

Figure 33: Simplified model of the double-dogleg test setup including two C50-style windows, with one serving as a reference (DL-135). Not shown are the coupling ports with RF feedthrough antennas located at the center of the broad walls close to the window on each end side.

The adapters are coupling only poorly to the structure to excite a standing field. The mode of excitation is a TE104 mode resonating around 1.5 GHz. Measuring the Q-value of the mode allows characterizing the RF losses of the cold RF window under test (the Q_0 is typically within 1e4-3e4), while the SRF losses in the Nb can be assumed as negligible in comparison. One dogleg/window assembly (DL-135) always serves as a reference standard against which all other dogleg/window assemblies will be tested[11]. The requirement for an RF window to pass the cold test was set to 2 W in a peak electrical field that is equivalent to that generated by a traveling TE_{10} mode carrying 5 kW in a waveguide of same

[11] DL-135 has been chosen as a reference since its RF window losses (P_{ref} = 1.07 W) are rather small as determined from several measurements carried out in permutation with two other dogleg/window assemblies.

cross-section. Given the power loss allowance of 2 W, a minimally achievable Q_0-value can be calculated based on the stored energy in the double-dogleg resonator scaled to the same peak field at the window location[12]. In turn, the actually measured Q_0 can be converted to the equivalent RF loss (P_{ref}) at 5 kW traveling power. This is plotted in Fig. 34 summarizing the experimental results of so far recorded C50 windows since 2008 (not in always chronological order). The serial number of the dogleg/window assembly under test is denoted next to the bars.

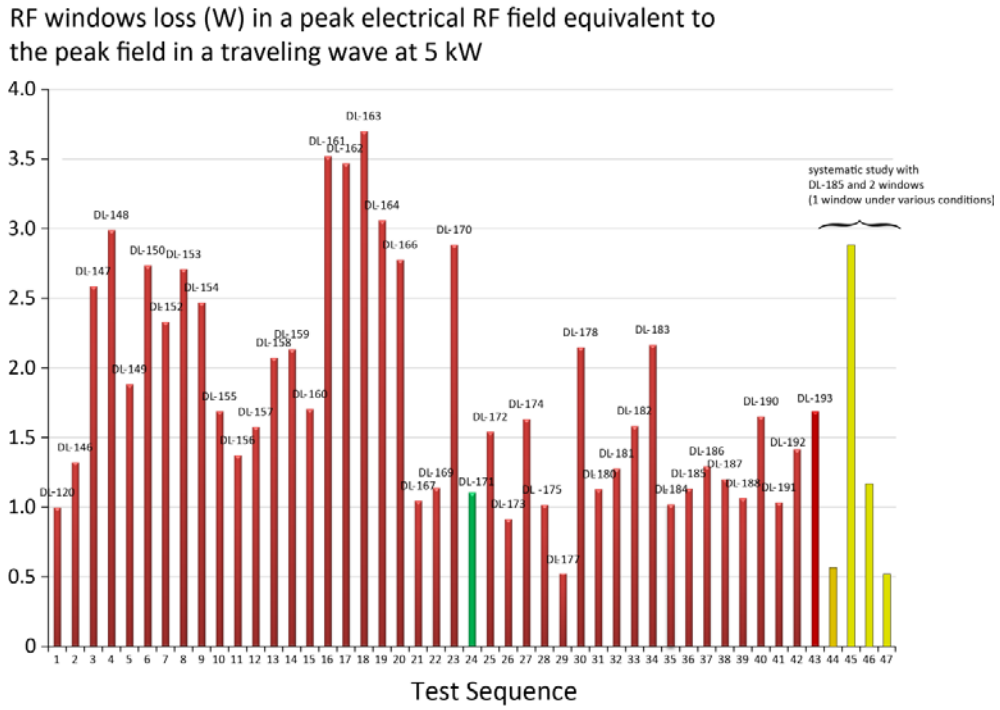

Figure 34: Individual RF power losses of C20/C50-style cold dogleg/RF window assemblies as evaluated from Q_0-measurements for a dedicated double-dogleg resonator immersed in liquid helium carrying the window under test together with a known reference dogleg/window assembly (DL-135). The RF power losses are scaled to the losses in a peak electric RF field equivalent to the peak field in a waveguide of same cross-section generated by a traveling TE_{10} mode carrying 5 kW power.

The RF power losses cover a range from P_{ref} = 0.51 W (DL-172) to P_{ref} = 3.7 W (DL-163) averaging at $\langle P_{ref} \rangle$ = 1.8 W. The reason for the strong variations cannot be fully determined. In some cases the measurements were performed at 2 K, for others at 4 K, which may change the NC losses in the window to some extent, though neither the conductivity of the metallization nor the loss tangent of the ceramic is assumed to change significantly from 4 K to 2 K, while the superconducting losses in the Nb enclosure should not contribute noticeably to the measured Q, which is on the order of 1e4.

However, there has been evidence in the past that losses in the window metallization play a crucial

[12] Given the cross-section, the TE10 cutoff frequency and the TE waveguide mode impedance at 1.5 GHz can be calculated readily. This allows determining analytically the electrical peak field in the waveguide of same cross-section for a traveling TE10 mode at 5 kW. In turn, for the same electrical peak field amplitude one can analytically estimate the associated stored energy of the TE104 mode in the double-dogleg setup based on its total length. Since this is strictly only applicable for a straight waveguide, the analytical estimates have been replaced with numerical findings for a model including the doglegs and windows.

role to impact the window losses. Already in 2008 we have carried out tests for this reason utilizing a then available non-metallized window made from ALON® as well as a standard alumina window with all metallization removed. Each of these windows were inserted (not brazed) in a standard Nb eyelet and just dropped into a dogleg. The corresponding losses were both slightly below P_{ref} = 0.1 W corresponding to a $Q_0 \approx 76000$. For metallized and brazed C20/C50 Alumina (Al995) windows however the losses are rarely smaller than P_{ref} = 1 W (Q_0 around 42000). For DL-171 marked green (test #24) at P_{ref} = 1.1 W (tested 2009) it has been reported that the metallization around the perimeter at the bottom of the ceramic was missing [33], which could be a reason for the comparably small losses. No history is known for other windows. Recent systematic studies have been carried out to find further correlations of losses attributable to the metallization (yellow bars in Fig. 34). First, an old unused, non-metallized C20 window (unknown material) has been recovered and dropped together with a Nb eyelet into a dogleg (DL-185) after removing the RF window from a previous test (test #36). This resulted in P_{ref} = 0.56 W (test #44), the 2nd lowest loss recorded in Fig. 34. In the subsequent test #45 a standard metallized window brazed to a Nb eyelet was dropped in the same dogleg resulting in P_{ref} as high as 2.9 W. Typically, some excess metallization and braze alloy may extend beyond the eyelet rim at the ceramic bottom (cf. Fig. 29 right). Grinding away this excess material and repeating the test for the same window (test #46) resulted in only P_{ref} = 1.2 W, which is a remarkable reduction. Eventually, a further test has been done with the same window after completely grinding away the eyelet portion at the bottom of the ceramic including the braze alloy and metallization underneath, which only leaves the lateral metallization with Nb eyelet intact. This resulted in only P_{ref} = 0.51 W (test # 47), the best result per Fig. 34 together with DL-177 (test #29)..

Given the strongly varying RF losses observed in cold windows in the frame of the VTA tests (by up to a factor ≈7.5), it is conceivable that cavity Q_0-values in cryomodules could be affected, though this depends also on the actual RF field amplitudes at the FPC's waveguide window position at discussed above. Given the varying boundary conditions during high power tests, the field amplitudes in the FPC waveguide at a given cavity stored energy may well vary for the following usual test conditions:

1) In the VTA for individual cavities (with close-to critically coupled top-hat adapter) or for cavity-pairs
2) In the Cryomodule Test Facility (CMTF) for high power acceptance tests with the FPC waveguide connected to the test klystron, but without stub tuners in place
3) In the CABAF tunnel, when the cavities are hooked up to the power transmission line including a stub tuner close to the klystron in the service buildings

For instance, after identifying the recipient cavities of the dogleg/window assemblies, the Q_0-values measured during commissioning have been associated to the individual losses (P_{ref}) reported above[13]. The findings are summarized in Fig. 35. The highest Q_0-values for the C75 cavities are associated with P_{ref} = 1 W (C75-001) and P_{ref} = 1.6 W (C75-003), respectively. The variation of the Q_0-values is relatively

[13] This correlation has been carried out for cavities carrying RF windows characterized in the double-dogleg resonator used first in CM C50-07, which excludes cavities in CM C50-01 through C50-06, but also a subset of cavities in CM C50-07. Some uncertainties remained in the correlation for a few cavities as database entries were ambiguous.

large for $P_{ref} \leq 2.2$ W such that a correlation of Q_0 with P_{ref} is not obvious in this regime. However, there is a more pronounced tendency that Q_0-values drop once $P_{ref} \geq 2.5$ W as indicated by the arrow. All results might still be affected by other loss mechanisms including stub tuner settings.

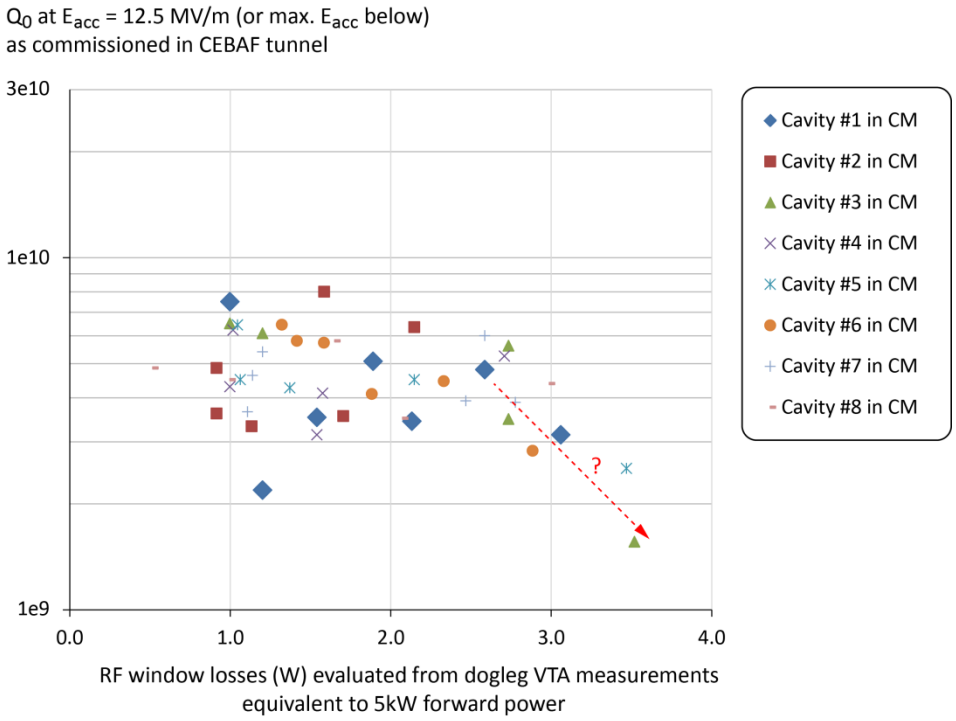

Figure 35: Q_0-values as measured at E_{acc} = 12.5 MV/m (or at the max. field achievable when cavity is limited below) at T = 2.07 K during CEBAF C50 cryomodule commissioning (CM-07 through CM-13) in dependence of the cold RF vacuum window losses (P_{ref}) as characterized individually in low power vertical Dewar tests. The colored symbols differentiate between cavity positions along the CM..

Note that despite a rejection criteria set for windows to not exceed P_{ref} = 2 W in the double-dogleg tests, all windows were apparently recycled and used in C50 cryomodules. We are now enforcing the quality control to reject lossy windows with P_{ref} > 2 W, which is substantiated by the findings in Fig. 35. More experimental investigations are necessary to determine the quantitative impact of RF window losses on the Q_0-performance of C20/C50 cavities. For instance, we propose to study the potential Q_0-variation of C50 cavities in dependence of stub tuner settings.

8. Cryomodule Commissioning Results of CM50-13 with first C75 LG Cavity Pair

By November 2017 CM50-13 has been commissioned in the CEBAF tunnel [34]. As discussed above, the new cavity shields were employed for the first time for all cavities. The RF performance results are summarized in Table 12. Except cavity IA345, all cavities have been limited by a quench. Both C75 cavities exhibited field emission radiation as was the case already during the cavity pair test in the VTA with yet no significant impact on the Q_0 value. The field emission in Cavity #1 cleaned up after additional RF processing and the cavity quenched at 19 MV/m. Compared to the VTA cavity pair tests, the Q_0-

values at E_{acc} = 12.5 MV/m degraded for all cavities as evaluated in Table 13.

Table 12: CM50-13 cryomodule commissioning results in CEBAF tunnel (north linac zone 13)

Cav. #	Cav. Type	Cav. SN	$E_{acc,max}$ MV/m	Q_0(2.07 K)[14] at E_{acc} = 12.5 MV/m	Q_{ext} FPC	Performance limit	FE onset MV/m
1	C75 HC *LG*	C75-001	19.0	8.0e9	1.3e7	Quench	-
2	C75 HC *LG*	C75-003	14.2	7.5e9	1.9e7	Quench	10.9
3	C50 OC *FG*	ia274	16.6	6.5e9	1.6e7	Quench	-
4	C50 OC *FG*	ia345	17.4	4.3e9	1.5e7	Waveguide vacuum	9.4
5	C50 OC *FG*	ia366	9.2	7.0e9*	1.6e7	Quench	-
6	C50 OC *FG*	ia351	14.0	5.8e9	9.8e6	Quench	-
7	C50 OC *FG*	ia038	16.9	6.0e9	1.3e7	Quench	-
8	C50 OC *FG*	ia260	15.5	4.5e9	7.4e6	Quench	7.3
average			15.3	6.2e9			

* at E_{acc} = 9.1 MV/m

Table 13: Unloaded quality factor measured at T = 2.07 K in VTA versus CEBAF tunnel during commissioning at E_{acc} = 12.5 MV/m

Cav. #	Cav. Type	Cav. SN	FE onset VTA MV/m	Q_0 VTA[15]	Q_0 CM commissioning[13]	Q_0 degradation VTA → CM %
1	C75 HC *LG*	C75-001	17.3	9.3e9	8.0e9	14.0
2	C75 HC *LG*	C75-003	9.9	8.1e9	7.5e9	7.4
3	C50 OC *FG*	ia274	16.3	9.6e9	6.5e9	32.3
4	C50 OC *FG*	ia345	-	8.6e9	4.3e9	50.0
5	C50 OC *FG*	ia366	-	7.8e9	limited at 9.1 MV/m	-
6	C50 OC *FG*	ia351	-	7.8e9	5.8e9	25.6
7	C50 OC *FG*	ia038	10.5	7.0e9	6.0e9	14.3
8	C50 OC *FG*	ia260	13.5	6.1e9	4.5e9	26.2
average				8.0e9	6.1e9	24.3

The least degradation has been observed for C75-003 with 7.4% followed by C75-001 with 14 %, both in presence of field emission. The table also comprises the FE onset field from the previous cavity pair VTA tests. Five cavities showed field emission radiation in the VTA, and four in the cryomodule. Except for cavity ia038, C50 cavities exhibited a significantly larger degradation than C75 cavities and up to 50% (ia345), though all CM-013 cavities have received identical measures for magnetic hygiene and shielding during refurbishment. The average Q_0(2.07K, 12.5 MV/m) for C50 cavities during commissioning (not accounting for ia366) is 5.5e9 (while 7.8e9 in the VTA), for the two C75 cavities it is

[14] The temperature of the cavity during cryomodule testing is not held constant at 2.07 K and the measured Q_0 is scaled to 2.07 K based on an assumed temperature-dependence of $Q_0(T)$.
[15] The Q_0 measurement error in the VTA is ~10%.

7.8e9 (while 8.7e9 in the VTA). On average the Q_0-degradation for C50 cavities is thus ≈30%, and only ≈11% for C75 cavities. This for instance could be the benefit of the *LG* material having a better flux expulsion efficiency than the *FG* material used in the old cavities. This is a promising finding, though the statistics is limited. For C50 cavities it was hoped to minimize the usual Q_0-degradation with the cavity magnetic shield in place that shall provide a shielding factor of ≈10 for magnetized components within the helium tank. Particularly the relatively large Q_0-degradation observed for the second C50 cavity pair (ia274 and ia345) cannot be understood without further analysis, while above discussed RF window losses could play an important role.

C75-001 has been equipped with three single-axis flux-gate magnetometers (serial numbers 1544, 1545, 1546) located inside the cavity magnetic shield and pointing in different directions to yield the information of all components of the remanent magnetic field at the cavity surface, as shown schematically in Fig. xx. The remanent field at this cavity was monitored during cryomodule assembly and it showed that the field components normal and transverse to the CM axis increased significantly after welding operations (Fig. xx). Improvements are necessary to both reduce stray field from the welding cables and to control the path of the welding current.

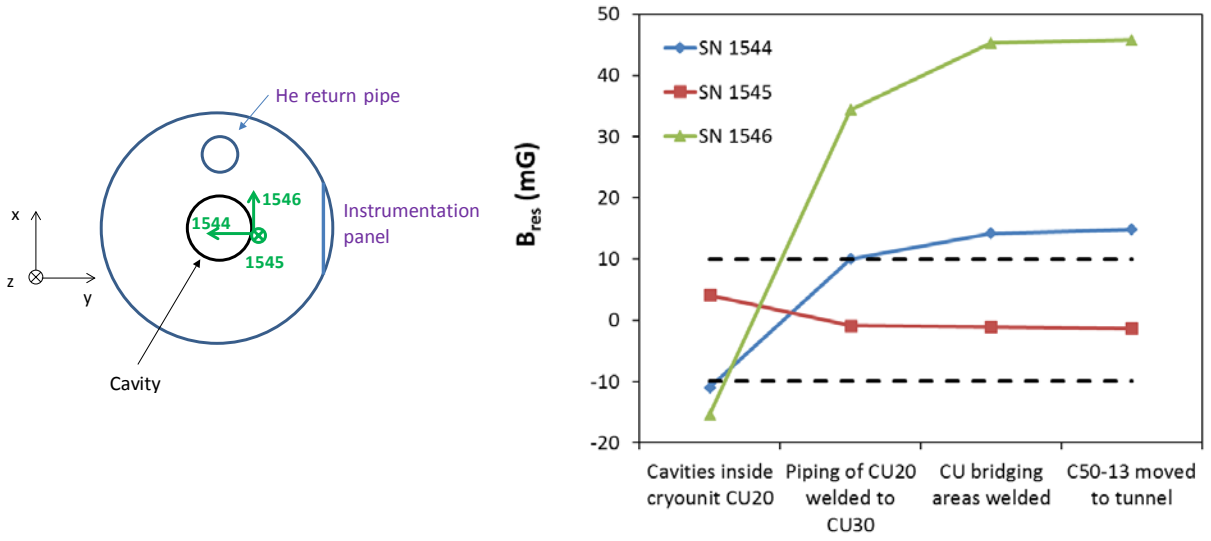

Figure xx: Schematic location of three flux-gate magnetometers on cavity 5C75-001 (left) and residual magnetic field measured during CM assembly (right).

All mechanical tuners in C50-13 were operated and the hysteresis recorded us usual during commissioning. No issues have been reported, which implies a verification of the earlier bench results for a C75 prototype.

The stub tuners have not been optimized at the time of commissioning, but used as set for previous cavities. For C75 cavities this resulted in Q_{ext}-values below but still rather close to the values of the individually tuned cavities on the bench (2e7). Specifically for C75-003 with the lowest Q_0-degradation an acceptable value of 1.9e7 has been achieved. For the C50 cavities however, the Q_{ext}-values are typically much higher (close to or beyond 1e7) than previously tuned on the bench (8e6 ± 1e6) except for ia260 with Q_{ext} =7.6e6. This raises the question whether the prevalent Q_0-degradation is caused by

RF window losses. As numerically evaluated above, a dramatic increase of RF losses in the metallization of the innermost, cold RF vacuum window may occur, when the FPC waveguide would be shortened at an unfavorable position. A stub tuner with the plungers already inserted strongly into the waveguide could create a comparatively strong standing wave component (high VSWR) such that the RF fields at the RF window position are causing elevated losses. It has therefore been proposed to repeat RF tests at a later date, particularly for ia345 when the stub tuner plungers are set flush with the inner waveguide wall. Such a test is useful to determine to what extent the stub tuner settings influence RF window losses – including dielectric/volumetric losses inside the ceramic – and thus have an impact on the Q_0-degradation observed.

9. Conclusion

The C75 program bears the chance to counteract the observed energy loss of cryomodules in CEBAF in order to maintain the 12 GeV energy reach of the machine. The major goal is to achieve an energy gain of 75 MeV per cryomodule, thus another boost of 50% compared to refurbished C50 cryomodules. The C75 program has been proposed in 2015 as the least invasive, least expensive modification to a C20 cryomodule by replacing the old Original CEBAF fine grain cavity cells with new large grain cells exhibiting a High Current cell profile (JLab prototyped design), while recycling as much of the cavity and cryomodule components as practically possible such as the FPC and HOM endgroups, helium tanks, cold RF windows, mechanical tuner components, and HOM 2 K waveguide absorbers, while replacement loads have been identified for the latter if needed. The geometrical benefit of utilizing the High Current cavity cell profile as a replacement of Original CEBAF cells has been quantified. The prospects of using large grain Nb for cavity production instead of fine grain Nb have been reviewed such as the expected lower surface resistance and better magnetic flux expulsion efficiency.

The proposed cavity modifications have been detailed. This for instance concerns alterations required to make the cavity compliant with the C20 mechanical tuner by using new end-cell holders to adapt to the new cell profile. Furthermore, a larger separation of the FPC waveguide to the cavity is conceived to obtain a higher external Q (2e7) – by design – than the C20/C50 cavities. This is in compliance with the 12 GeV physics program at up to 460 µA average beam current. Supported by numerical simulations, the larger separation also reduce RF losses in the waveguide, while the impedances of all crucial dipole HOMs – including those that require the FPC waveguide as a HOM coupler – can be kept below the machine's BBU impedance threshold.

The energy gain of 75 MeV equates to an accelerating field of nominally 19.07 MV/m per cavity, which also requires an upgrade of the original 5 kW to 8 kW RF system zones. This upgrade is not associated with major risks since the required 8 kW RF system is principally identical with that already operating for the R100 (C100-type) injector cryomodule. The proper heat stationing of the FPC waveguide in C75 cavities to adapt to the higher power levels is yet under investigation. The nominal accelerating field – plus a conceived contingency margin of 7.5% – can be sustained with the available generator power. This takes into account waveguide attenuation through the transmission line with estimated 7 kW of usable input power left at the cavity entrance in presence of up to 31 Hz microphonic cavity detuning. The associated dynamic heat load ($\sim E_{acc}^2$) expected for C75 cryomodules at the specified cavity Q_0-value of 8e9 at 2.07 K is within the cryomodule heat load capacity and deemed supportable by

the central helium liquefier plants.

Three C75 prototype cavities have been recently produced at JLab to investigate the associated risks involved with the proposed modifications. The endgroups of C20 spare cavities have been salvaged for these cavities and welded to the HC cells. The two best-performing cavities (C75-001, C75-003) – as determined in individual VTA tests – have been subsequently installed as a cavity-pair in the refurbished cryomodule C50-13 among six standard C50 cavity pairs. C50-13 has been commissioned in the CEBAF tunnel by Nov. 2017 (skipping acceptance tests in the cryomodule test facility due to time constraints). It has been found that the Q_0-value of the two C75 cavities degraded by only ≈1/3 compared to the average degradation observed for C50 cavities. This resulted in the highest Q_0-values achieved among all so far refurbished cavities. The Q_0-values at 2.07 K were 8e9 for C75-001 and 7.5e9 for C75-003 at E_{acc} = 12.5 MV/m and did not deteriorate – within error bars – up to the quench field limit. The nominal accelerating field of 19.07 MV/m was marginally achieved in one cavity only, but these results were expected from prior VTA tests. The quench sites had been located by optical inspections and are associated with defects at cavity equators from electron beam welds. The avoidance of weld issues is currently addressed in house, however it is recommended to contract the production of C75 cavities to vendors with state-of-the-art fabrication facilities.

No issues were reported when operating the mechanical tuners of the C75 cavities with the modified cell holders [36]. This indirectly validates that the mechanical stiffness of the C75 cavities is comparable to that of C50 cavities after adding stiffening rings and agrees with earlier bench tests for a C75 prototype and a C50 cavity with and without the cavity magnetic shield installed.

Furthermore, microphonic measurements for CM-13 cavities have shown that the peak detuning levels (6σ) in C75 prototype cavities were slightly below the specified allowance of 30 Hz during the measurement period. Overall, the microphonic peak detuning levels were similar to those measured for C50 cavities, which would sustain an operation up to 20.5 MV/m. Potential sporadic microphonic detuning excursions above the peak detuning allowance are estimated to trip cavities at an acceptable rate of one RF trip per day. The benefit of the additional support brackets installed on the HOM waveguide elbows (only for C75 cavities in C50-13) to suppress low-frequency mechanical modes associated with swinging motions of the C20 HOM waveguides could not be further elaborated based on the present microphonic measurements.

The prevalent Q_0-degradation of C50 cavities and to minor extent for C75 cavities is still not fully understood given that cavity magnetic shields were installed to suppress the magnetic field at the cavity surface to nominally 10 mG. Degaussing of the whole cryomodule vessel as routinely implemented for LCLS-II cavities is foreseen in the future [37]. RF losses arising from the 2 K RF vacuum window however, specifically due to the normal-conducting metallization on the ceramic perimeter, could yield a yet unquantified heat load into the helium bath observable as a Q_0-degradation. Past and recent systematic studies on individual RF windows in the VTA showed a significant correlation between the measured losses and the amount of metallization present on the window. The VTA results also revealed that the RF losses among C20/C50 windows can vary by up to a factor of 7.5. A tendency has been found that very lossy windows (P_{ref} > 2.5 W) as individually characterized in the VTA with a dedicated setup degrade the Q_0-values of refurbished C50 cavities as commissioned in the CEBAF tunnel in accordance with the loss, though more experimental investigations are required to verify this claim. Numerical simulations have clearly indicated though that such losses can depend strongly and sensitively on actual plunger settings

of an external stub tuner. Such stub tuners are routinely employed at CEBAF to fine tune the external Q of the FPC in order to minimize the required generator power. The computations revealed that dramatic RF losses may occur in the window metallization when the external Q is tuned to lower values. This principally agrees with the observation in CEBAF that a reduction of the external by merely a factor of two usually leads to excessive heating at the RF window as verified with infrared sensors. It is proposed to study whether the stub tuner settings in CM-13 are fact related to observed Q_0-degradations (up to 50 % in cavity ia345) in future measurements.

In conclusion, the CEBAF commissioning results for a C75 prototype cavity-pair among six C50 cavity pairs in C50-13 have been promising despite known fabrication issues for the C75 cavities. A new mark has been set by achieving the highest Q_0-values among all so far refurbished cavities. The C75 program is therefore proceeding well. Two further C75 cavities will be built in house, while it is conceived to order a full set of eight C75 cavities from industry.

At the rather high accelerating fields, field emission is a common concern in SRF cavities, particularly in CW operation as presently experienced for C100 cavities. The field emission can only be eliminated by establishing stricter clean-room protocols for assembly procedures. Concerning field emission, the C20 cryomodules have two benefits over C100 cryomodules by design, which could become important during operation. Firstly, the cavity-pair inner adapters exhibit only a small inner diameter (1.5”), which will collimate a portion of the field-emitted electrons at rather low impact energies before entering the adjacent cavities. This will reduce the severity of activated beam line components. Secondly, the interconnecting beam tube distance is a half-integer number (2.5) of cell lengths ($c/2f$). This can significantly suppress the field emission in upstream direction for the electrons yet being accelerated to neighboring cavities as cavities are out of phase for continuous, maximal energy gain unlike in downstream direction [38].

10. C75 Cavity Design Parameters and RF Specifications

All above discussed and essential C75 cavity design parameters and RF specifications are eventually summarized in the tables below for future reference.

Table 18: C75 Cavity Design Parameters

Parameter	Unit	Value	Comments
Number of cavity cells		5	
L_{act}	mm	491.6 ± 3	
Cavity installation length	mm	721.36e ± 2	Controlled by customized beam tube on HOM endgroup side
R/Q	Ω	525.4	$U_{eff}^2/(\omega * W)$
R/Q per cell	Ω	105.1	
G	Ω	275.6	
R/Q·G	Ω^2	144805	
R/Q·G per cell	Ω^2	28961	
√(R/Q)/L_{act}	√Ω/m	46.63	
E_{pk}/E_{acc}		2.45	
B_{pk}/E_{acc}	mT/(MV/m)	4.18	
k_{cc}	%	3.12	
Tube ID	mm	70	
Iris ID	mm	70	
TE_{11} tube cutoff	GHz	2.51	
TM_{01} tube cutoff	GHz	3.28	
TE_{10} FPC cutoff	GHz	1.1	
TE_{10} HOM waveguide cutoff	GHz	1.9	

Table 19: C75 RF Specifications

Parameter	Unit	Value	Comments
Energy gain per CM	MeV	75	80.6 MeV with 7.5% contingency
Operating RF frequency f_0	MHz	1497	with cavity under compression
Operating temperature	K	2.07	29 ± 0.1 Torr nominal helium pressure
Number of cavities per CM		8	
Maximum beam current	µA	460	
Microphonic detuning δf (rms)	Hz	5	
Microphonic detuning δf (peak)	Hz	30	
E_{acc}	MV/m	19.07	U_{eff} = 9.375 MV, E_{pk} = 46.6 MV/m, B_{pk} = 79.7 mT (δf = 38.6 Hz max . allowable)
$E_{acc,max}$ (E_{acc} +7.5%)	MV/m	20.5	U_{eff} = 10.08 MV, E_{pk} = 50.1 MV/m, B_{pk} = 85.7 mT (δf = 31 Hz max . allowable)
Maximum beam loading	kW	4.3	*At* E_{acc} = 19.06 MV/m 4.6 kW at E_{acc} = 20.5 MV/m
Remanent magnetic field in CM at cavity position	mG	10	After cryomodule degaussing (absolute field)
Allowable RF window losses	W	≤ 2	As measured in special setup in Dewar at 2 K (low power) and extrapolated to 5 kW forward power
Q_0		8e9	up to E_{acc} = 19.07 MV/m
P_c	W	20.9/24.2	for E_{acc} = 19.07/20.6 MV/m at Q_0 = 8e9
P_g	kW	8	
P_g usable	kW	7	assuming 0.6dB attenuation in transmission line from klystron
Q_{ext} FPC		2e7 ± 15 %	adjustment to high Qext-values possible by WR650 stub tuning
Resonant bandwidth ($f_0/2\cdot Q_l$)	Hz	37.5	
Q_{ext} field probe		0.8-1.8e12	
HOM dipole impedances R_{tr}	Ω/m	≤ 2e10	$R_{tr} = R/Q(r)\cdot Q_{l\_HOM}/k\cdot r^2$ BBU impedance threshold is 2e10 Ω/m for 12 GeV baseline physics with 460 µA max., stretched goal is 1e10 Ω/m
Warm target RF frequency	MHz	1494.6 ± 75 kHz	T = 300 K, *r.H.* = 40%, *P* = 1 atm
VTA target RF frequency	MHz	1497.3 ± 100 kHz	*T* = 2.07 K, *P* ≤ 1e-7 mbar
Tuning sensitivity $\Delta f/\Delta z$	MHz/mm	470 ± 80	with cavity magnetic shield based on bench measurements
Lorentz Force Detuning	Hz/(MV/m)^2	-2 to -3	
Pressure sensitivity $\Delta f/\Delta P$	Hz/Torr	-187 ± 9	Based on VTA measurements
FE onset field	MV/m	≥ 19.5	defined to be the first E_{acc} where the measured radiation level is ≥ 0.01 mR/hr (measured inside Dewar lid)

11. References

[1] M. Drury et al., "Summary Report for the C50 Cryomodule Project", TUP108, Proc. PAC 2011, New York, NY, USA, 2011.

[2] A. Freyberger, "Technical and Economical Motivation", Mini-workshop on beam-line field-emitter particulates in CEBAF SRF linacs, JLab, 29. February 2016.

[3] H. Wang, F. Marhauser and R. Rimmer, "Simulations and Measurements of a Heavily HOM-Damped SRF Cavity", WEPMS070, Proc. PAC'07, Albuquerque, New Mexico, USA, 2007.

[4] F. Fors, "C75 – C50 Comparative Sensitivity and Modal Analysis", Mechanical Engineering Note, 5/2/2016.

[5] G. Ciovati, G. Cheng, F. Fors, J. Fisher, D. Forehand, J. Henry, F. Marhauser, M. McCrea, E. Daly, and R. Rimmer, "Tuning sensitivity and stiffness of C20/C50 and C75 cavities", JLab Technical Note, 03/04/2017.

[6] F. Fors, "C75 Cavity – Full cavity assembly modal analysis", Technical Note, 6/7/2016.

[7] G. Cheng, "C50 and C75 Cavity Pair Experimental Modal Analysis Plan, Technical Note, 3/2/2017.

[8] F. Marhauser et al., "Status and test Results of High Current 5-cell SRF Cavities Developed at JLab", MOPP140, Proc. EPAC'08, Genoa, Italy, 2008.

[9] F. Marhauser et al., "Critical Dipole Modes in JLab Upgrade Cavities", THP009, Proc. LINAC'10, Tsukuba, Japan, 2010.

[10] F. Marhauser, "JLab SRF Cavity Fabrication Errors, Consequences and Lessons Learned", MOPC115, Proc. IPAC2011, San Sebastian, Spain, 2011.

[11] H. Wang, "Analytical Design of a Waveguide Iris/Stub Tuning Coupler to an Overcoupled Superconducting Cavity", Proc. PAC'13, Shanghai, China, 2013.

[12] H. Wang, "A MathCAD Program to Calculate the RF Waves Coupled from a WR650 Three-Stub Tuner to a CEBAF Superconducting Cavity", JLab Technical Note JLAB-TN-04-031, 2004.

[13] Tom Powers, private communication.

[14] Roland Overton, private communication.

[15] F. Marhauser, "Calculations for RF Cavities with Dissipative Material", Proc. of the 2015 SRF Conference, THPB003, Whistler, Canada, 2015.

[16] K. Davis, T. Powers, "SL20 Microphonic Testing", Internal Note, JLab, Feb. 2005.

[17] G. Krafft, I. Shin, and B. Yunn, "Revised Specification for HOM Damping in 12 GeV Accelerating Cavities", JLab technical Note, JLAB-TN-09-015, Newport News, USA, 2009.

[18] F. Marhauser, "Next Generation HOM-damping", Supercond. Sci. Technol. 30 (2017) 063002, (38pp), https://doi.org/10.1088/1361-6668/aa6b8d

[19] F. Marhauser, R.A. Rimmer, K. Tian, and H. Wang, "Enhanced Method for Cavity Impedance Calculations", FR5PFP094, Proc. IPAC2009, Vancouver, Canada, 2009.

[20] G. Cheng, private communication (total heat capacity is 256 Watts per cavity).

[21] W. Singer et al., "Development of large grain cavities", Phys. Rev. ST Accel. Beams 16, 012003, 2013.

[22] G. Ciovati, P. Dhakal, and G. R. Myneni, "Superconducting radio-frequency cavities made from medium and low-purity niobium ingots", Supercond. Sci. Technol. 29 (2016) 06002, 2016.

[23] G. Ciovati, P. Dhakal, P. Kneisel, and G. R. Myneni, “Summary of performance of superconducting radio-frequency cavities built from CBMM niobium ingots”, Ingot Niobium Summary, Virginia, USA, Volume: AIP CP 1687, 2015.
[24] G. Ciovati, P. Dhakal, P. Kneisel, J, Spradlin, and G. R. Myneni., “RF performance of ingot niobium cavities with medium-low purity”, MOPB001, Proc. of SRF2015, Whistler, BC, Canada, 2015.
[25] G. Ciovati et al., “Experience with the fabrication, processing and testing of the prototype “C75” 5-cell cavities”, JLab Technical Note, May 17, 2017.
[26] G. Ciovati, P. Kneisel and G. R. Myneni, “America’s overview of superconducting science and technology of ingot niobium”, in Proc. of the Symposium on the Supercond. Sci. and Technol. of Ingot Niobium, AIP Conf. Proc. 1352, 2011, p. 25, 2011.
[27] G. Cheng, E. Daly, “C50 Cryomodule Magnetic Shielding Design and Analysis”, JLab Technical Note, JLAB-TN-08-072, 2008.
[28] G. Ciovati, “Magnetic Hygiene: Results and Planning”, C75 Preliminary Design Review, JLab, Newport News, Jan. 21st 2006.
[29] G. Ciovati, G. Cheng, M. Drury, J. Fischer, and R. Geng, “Impact of remanent magnetic field on the heat load of original CEBAF cryomodule”, IEEE Transactions on Applied Superconductivity, DOI: 10.1109/TASC.2016.2631938, Nov. 2016.
[30] S.J. Zinkle, R.H. Goulding, “Loss Tangent Measurements on Unirradiated Alumina”, Technical Report, Oak Ridge National Lab, DOE/ER--0313/19; 1995, 231-234.
[31] N. MnN Alford et al., “Dielectric loss of oxide single crystals and polycrystalline analogues from 10 K to 320 K”, Journal of the European Ceramic Society 21 (2001), 2605-2611.
[32] Brookhaven National Laboratory Selected Cryogenic Handbook, Volume II, BNL-10200-R, Vol. II, 1980.
[33] Scott Williams, private communication.
[34] M. Drury, “C50-13 Commissioning Summary”, Meeting Slides, 13th Nov. 2017.
[35] Gary Cheng, private communication.
[36] Mike Drury, private communication.
[37] G. Cheng, G. Ciovati, B. Legg, “C50-13 Degaussing Experiments”, Technical Note, Dec. 2016.
[38] F. Marhauser, S.V. Benson, D.R. Douglas, “Suppression of Upstream Field Emission in RF Accelerators”, MOPB061, Proc. of SRF 2015, Whistler, Canada, 2015.